Interplay of charge noise and coupling to phonons in adiabatic electron transfer between quantum dots

Jan A. Krzywda* and Łukasz Cywiński
Institute of Physics, Polish Academy of Sciences, al. Lotników 32/46, PL 02-668 Warsaw, Poland

(Received 21 April 2021; revised 16 July 2021; accepted 22 July 2021; published 20 August 2021)

Long-distance transfer of quantum information in architectures based on quantum dot spin qubits will be necessary for their scalability. One way of achieving this goal is to simply move the electron between two quantum registers. Precise control over the process of shuttling such a single electron through a chain of tunnel-coupled quantum dots is possible when interdot energy detunings are changed adiabatically. The deterministic character of shuttling is, however, endangered by the open nature of the system, as the transferred electron is coupled to thermal reservoirs: sources of fluctuations of electric fields and lattice vibrations. We present a comprehensive analysis showing how the electron transfer between two voltage-controlled quantum dots is affected by electron-phonon scattering and interaction with sources of $1/f$ and Johnson charge noise in both detuning and tunnel coupling. The electron-phonon scattering turns out to be irrelevant in Si quantum dots, with charge noise dominating the dynamics of the system at slow detuning sweep, when the electron spends more time delocalized between the dots (i.e., near the anticrossing of the tunnel-coupled states). Competition between the effects of charge noise and the Landau-Zener effect leads to an existence of an optimal detuning sweep rate, leading to minimal probability of leaving the electron behind. In GaAs quantum dots, on the other hand, piezoelectric coupling to phonons is strong enough to make the processes of interdot transfer assisted by phonon emission and absorption dominate over transitions caused by charge noise. The probability of leaving the electron behind then depends monotonically on detuning the sweep rate over a broad range of rates, and values much smaller than in silicon can be obtained for slow sweeps. However, after taking into account limitations on transfer time imposed by the need for preservation of a shuttled electron's spin coherence, the minimal probabilities of leaving the electron behind in both GaAs- and Si-based double quantum dots turn out to be of the same order of magnitude. Bringing them down below 10^{-3} requires temperatures $\leqslant 100$ mK and tunnel couplings above 20 μeV.

DOI: 10.1103/PhysRevB.104.075439

I. INTRODUCTION

In quantum computing architectures based on voltage-controlled quantum dots (QDs) developed in GaAs/AlGaAs [1–3], Si/SiGe [4], and Silicon-Metal-Oxide-Semiconductor (SiMOS) [5–8] structures, scalability will be possible only if quantum information is transferred between few-qubit registers, separated by distances much larger than the typical QD size. This is caused by the short-distance character of the exchange interaction needed for two-qubit gates and the spatial extent of wiring needed for controlled application of voltages to the gates defining the dots, which together put limits on density of a qubit array [9]. Coupling of electron spins to microwave photons is a possible mean of coherent coupling of spin qubits in GaAs [10] and silicon [11–14]. A conceptually simpler alternative, which has been recently pursued in experiments [15–27], is to simply transfer an electron spin qubit over a large (at least a few micrometer) distance.

We focus here on electron transfer along a chain of tunnel-coupled QDs [21–27]. The shuttling is then caused by controlled tilting of energy levels of neighboring QDs that makes an electron move from one dot to the other. The basic step in such a process is single electron transfer between two tunnel-coupled QDs. In a simplified situation, in which we neglect spin and valley (in the case of Si) degrees of freedom of the electron, the basic physics is captured by the Hamiltonian acting in a two-dimensional Hilbert space spanned by $|L(R)\rangle$ states, corresponding to electron localized in a local ground states of energy $E_{L(R)}$ in left (right) dots,

$$\hat{H} = \frac{\epsilon}{2}\hat{\sigma}_z + \frac{t_c}{2}\hat{\sigma}_x\,, \tag{1}$$

where $\epsilon = E_L - E_R$ is the so-called interdot detuning of energy, t_c is the tunnel coupling between the QDs, $\hat{\sigma}_z = |L\rangle\langle L| - |R\rangle\langle R|$ and $\hat{\sigma}_x = |L\rangle\langle R| + |R\rangle\langle L|$. For $\epsilon \ll -t_c$, the lowest energy state is localized in the L dot, and this is the state that we take as an initial one in all the considerations below. For $\epsilon \gg t_c$, the lowest-energy state is localized in the R dot and one, of course, expects that for a very slow change of ϵ from negative to positive values, the evolution will be adiabatic and

*krzywda@ifpan.edu.pl

the system will end up in this state. For a linear sweep, $\epsilon \propto v\tau$, where v is the rate of change of detuning, and constant t_c, we are dealing with a classical Landau-Zener (LZ) model [28], for which the probability of having the electron in an excited state for $\epsilon(\tau) \to \infty$ (i.e., leaving the electron behind in the L dot) is given by

$$Q_{\mathrm{LZ}} = \exp\left(-\pi t_c^2/2v\right), \tag{2}$$

so a near-perfect adiabatic transfer occurs when $t_c^2/v \gg 1$, i.e., when the sweep rate is low.

Changing the interdot detunings slowly is thus an obvious way to perform an on-demand deterministic transfer of an electron spin qubit. Of course, the total shuttling time should be much shorter than the spin coherence time of a moving electron, and according to Eq. (2) this requirement will put a lower bound on values of t_c characterizing the chain of QDs. However, another issue needs to be addressed before we can claim to have a realistic estimate of sweep rate v giving the smallest possible probability of error Q in transfer between a pair of dots. Electrons are affected by charge noise unavoidable in semiconductor nanostructures and coupled to lattice vibrations. As we show in this paper, interactions with sources of electric field noise and phonons in realistic Si- and GaAs-based structures are dominating the physics of charge transfer in a wide range of sweep rates, with nonadiabatic effects described by the LZ theory being relevant only for very fast sweeps.

Since our focus here is on the open system character of an electron tunneling between two QDs, we use the above-described simplest possible two-level model of the closed system. Taking into account the spin degree of freedom and spin-orbit coupling that affects its dynamics during the electron motion in GaAs [29] (and to a smaller extent in silicon [29,30]), and then a valley degree of freedom in Si [31–33], leads to four- or eight-level models with multiple anticrossings of states [29,30,34–40]. The two-level model used here exhibits a simpler behavior in the closed system case, and using it will typically lead to an underestimation of unwanted effects due to not-slow-enough sweeps (for a closed system) and coupling to environment (for an open system). The results given in this paper consequently correspond to the best-case scenario for given t_c and assumed magnitudes of charge noise and temperature.

The physics of the LZ effect in presence of coupling to environment has obviously been a subject of multiple works. Dissipative adiabatic evolution affected by coupling to bosonic baths having Ohmic spectrum was most often considered [41–46]. It is known [47,48] that coupling to a zero-temperature bath suppresses the final occupation of the higher-energy state (the electron being left behind in the initial dot in the physical scenario of interest here), while at finite temperature this occupation can be enhanced [42,49–52], which for the weak coupling leads to a nonmonotonic occupation of the excited state as a function of the rate of change of the adiabatic parameter [53]. Additionally, coupling to low-temperature reservoirs were discussed in many physical contexts [41,54,55]. Stochastic modifications of LZ parameters were also considered [56–58], including fast classical fluctuations [59] and noise characterized by nontrivial spectral density [38,60–63], including $1/f$-type noise, the tail of which also resulted in incoherent transitions between the states [38,64,65]. In this paper, we focus on QDs based on silicon and GaAs and employ realistic models of charge noise (having both Johnson/Ohmic and $1/f$-type spectra, and coupling to both ϵ and t_c) and phonon interaction with an electron confined in a double QD. We use the adiabatic master equation (AME) [41,52,66] in which the influence of the environment (actually a few distinct reservoirs in the case discussed here) is modeled with energy-dependent rates of transitions between instantaneous eigenstates of the slowly changing Hamiltonian of the system. For negligible probability of coherent LZ excitation, this approach reduces to a simple differential rate equation [67,68]), which we solve in a way analogous to the one described in Ref. [52].

During the detuning sweep, the energy gap between eigenstates of instantaneous Hamiltonians varies between $t_c \sim 10\ \mu$eV and the largest value of $\epsilon \sim 1$ meV. With temperatures in experiments typically around 100 mK, corresponding to thermal energy of $\approx 10\ \mu$eV, we should expect a nontrivial role of temperature dependence of rates of energy absorption and emission by the reservoirs. Note that in our previous work [38], we focused on the influence of *classical* (i.e., high-temperature) $1/f$ charge noise on electron transfer. Here we address the situation of lower temperatures/larger tunnel couplings, taking into account the quantum limit [69] of both $1/f$ noise from two-level fluctuators (TLFs) present in the nanostructure and Johnson noise from reservoirs of free electrons, while furthermore considering the coupling of the moving electron to phonons. Coupling to all these thermal reservoirs gives transition rates, $\Gamma_{+/-}(\Omega)$ for transfer of energy Ω from/to the environment, that nontrivially depend on Ω. The detailed balance between them, which reads $\Gamma_+/\Gamma_- = e^{-\beta\Omega}$, has the following general consequence for the dynamics of the system. With the system initially in the ground state, transitions into an excited state are exponentially suppressed for large negative detunings, and they start to become increasingly efficient as we approach the anticrossing of levels, at which the gap is minimal and equal to t_c. This effect of enhancement of the excitation rate at the anticrossing is additionally strengthened in the considered system by the fact that an electron delocalized between the two dots is more susceptible to both charge noise and interaction with phonons (as the transitions between states localized in each dot that govern the dynamics in far-detuned regimes are suppressed by a small overlap of wave functions). The finite occupation of the wrong dot generated during passing through $|\epsilon| \lesssim t_c$ region can then be diminished ("healed" in the terminology used below) by processes of energy emission into the reservoirs that dominate over processes of energy absorption by them when $\epsilon \gg k_B T$. Arriving at the final result of interplay between environment-induced excitation near the anticrossing and the subsequent energy relaxation (the environment-assisted dissipative tunneling into the correct final state), requires consideration of realistic coupling to all the reservoirs at temperatures and sweep rates relevant for experiments in QDs. Such careful consideration is the goal of this paper.

Our key qualitative result concerning application to realistic QDs is that in Si-based structures (both Si/SiGe and SiMOS) the dominant process disturbing the adiabatic

evolution close to anticrossing of levels is due to charge noise (with coupling to phonons giving transition rates three orders of magnitude smaller than those estimated for charge noise), and the finite probability of leaving the electron behind is subsequently diminished by relaxation processes due to charge noise and phonons that occur at large detunings only when the transfer is very slow. Competition between the LZ process, incoherent excitation close to the anticrossing, and relaxation at large detuning results in nomonotonic dependence of occupation of the excited state (the electron left behind in the wrong dot) on the detuning sweep rate, similar to one obtained in Ref. [53]. On the other hand, in GaAs/AlGaAs structures the piezoelectric coupling to phonons dominates over coupling to charge noise over a wide range of detunings and, consequently, the processes involving energy exchange between the transferred electron and lattice vibrations dominate the physics of the problem. The longer the charge transfer takes, the more time the system spends in the far-detuned regime in which the energy gap exceeds thermal energy, and the closer it gets to a thermalized state characterized by small occupation of higher-energy levels, i.e., of the electron being in the wrong dot. Phonons thus help in effecting the interdot charge transfer. These conclusions are quite robust against modifications of parameters of high-frequency properties of Johnson and $1/f$-type charge noises considered here.

The paper is organized in the following way: In Sec. II, we set up the problem for the closed system and discuss the adiabatic condition for its dynamics, introduce the AME as an approach to open system dynamics, and discuss a few physically transparent (and, as we show later, relevant for the case of electron transfer in silicon- and GaAs-based QDs) approximate solutions of this equation. In Sec. III, we calculate the detuning-dependent transition rates between instantaneous eigenstates of the two-level Hamiltonian. We perform calculations for coupling to phonons and finite-temperature environments that cause charge noise of both Johnson and $1/f$ types in detuning and tunnel coupling. We give there a discussion of expected amplitude of $1/f$ noise at GHz frequencies relevant for transitions during electron transfer in realistic GaAs- and silicon-based QDs. Finally, in Sec. IV we use these rates to calculate the dynamics of the electron driven adiabatically through an anticrossing of levels associated with the two dots and show a qualitative difference between resulting probability of leaving the electron behind between GaAs- and silicon-based QDs. In the last section, we discuss some of the implications of these results for experimental efforts aimed at using chains of QDs for coherent shuttling of electron spin qubits.

II. MODEL OF SYSTEM DYNAMICS

A. Adiabatic condition for closed system

We consider two energy levels that in the double QD case correspond to the lowest-energy orbital states localized in each of the two dots, $|L\rangle$ and $|R\rangle$. In case of silicon QDs, we assume that the valley splitting ΔE_V is large enough for us to consider a single anticrossing of two lowest-energy valley-orbital levels. It should be noted that if a state traverses this anticrossing in a diabatic way (due to LZ physics or the influence of noise that we discuss at length here), in the presence of interface disorder activating inter-valley tunneling t_c' between the dots, at $\epsilon = \Delta E_V$ a second anticrossing appears [30,35,39]. An effectively adiabatic passage through this anticrossing would correct the charge-transfer error incurred at the first anticrossing, but at the price of the electron appearing in the R dot in an excited valley state. Such a stochastic transition between ground and excited valley states will pose problems for charge and spin shuttling across many dots. These, however, will be further discussed elsewhere [70].

We also neglect the spin degree of freedom—interplay between the nonadiabatic effects in charge transfer and dynamics of the spin of the transferred electron will be discussed elsewhere [70] (an exception is made in Sec. V when considerations on spin dephasing due to quasistatic noise in spin splitting are invoked to limit the realistic detuning sweep rates from below). Our neglect of spin-orbit-activated tunnel coupling between states with opposite spin projections [30,34,35,39] is more justified for Si than for GaAs, but our focus here is on charge transfer dynamics, with the spin transfer aspect of the problem playing a limited role. We therefore work with the model defined by the Hamiltonian from Eq. (1), in which we now assume that ϵ and t_c depend on time τ.

For any value of $\epsilon(\tau)$ and tunnel coupling $t_c(\tau)$, the Hamiltonian $\hat{H}(\tau)$ has eigenstates

$$\begin{aligned} |+,\theta(\tau)\rangle &= \cos[\theta(\tau)/2]|R\rangle + \sin[\theta(\tau)/2]|L\rangle, \\ |-,\theta(\tau)\rangle &= \cos[\theta(\tau)/2]|L\rangle - \sin[\theta(\tau)/2]|R\rangle, \end{aligned} \tag{3}$$

where $\theta(\tau) = \mathrm{arccot}(-\epsilon(\tau)/|t_c(\tau)|)$. The energies of these states are plotted as a function of interdot energy detuning ϵ in the top panel of Fig. 1. The discussion of nonadiabatic effects due to time dependence of ϵ and t_c, or effects of interaction with the environment, is most transparent if we transform the state of the system into an adiabatic frame [71]: Instead of working with $|\psi(\tau)\rangle$ which fulfills $i\partial_\tau|\psi(\tau)\rangle = \hat{H}(\tau)|\psi(\tau)\rangle$, we work with $|\tilde{\psi}(\tau)\rangle \equiv \hat{U}[\theta(\tau)]|\psi(\tau)\rangle$, where a time-dependent unitary operator,

$$\hat{U}[\theta(\tau)] = \exp[i\hat{\sigma}_y\theta(\tau)/2], \tag{4}$$

transforms the R/L states into the instantaneous eigenstates of $\hat{H}(\tau)$: $|+(-),\theta(\tau)\rangle = \hat{U}[\theta(\tau)]|R(L)\rangle$. One can see that for a perfectly adiabatic evolution of the system, for which an initial superposition of eigenstates of $\hat{H}(\tau_i)$ at given τ_i evolves into *the same* superposition of eigenstates of $\hat{H}(\tau_f)$ at the final time τ_f, the transformed $|\tilde{\psi}(\tau)\rangle$ state is *time independent*. Indeed, the evolution in the adiabatic frame is controlled by

$$\hat{\mathcal{H}}(\tau) = \hat{U}[\theta(\tau)]\hat{H}(\tau)\hat{U}^\dagger[\theta(\tau)] - i\hat{U}[\theta(\tau)]\left(\frac{\partial\hat{U}^\dagger[\theta(\tau)]}{\partial\tau}\right), \tag{5}$$

which for the system discussed here reads

$$\hat{\mathcal{H}}(\tau) = \frac{\Omega(\tau)}{2}\hat{\varsigma}_z - \frac{\dot{\theta}(\tau)}{2}\hat{\varsigma}_y, \tag{6}$$

where $\hat{\varsigma}_z$, $\hat{\varsigma}_y$ are Pauli operators in $|+,\theta(\tau)\rangle$, $|-,\theta(\tau)\rangle$ basis of instantaneous eigenstates of the time-dependent Hamiltonian $\hat{H}(\tau)$, $\dot{\theta} = d\theta(\tau)/d\tau$, and the instantaneous energy splitting is

$$\Omega(\tau) = \sqrt{\epsilon^2(\tau) + t_c^2(\tau)}. \tag{7}$$

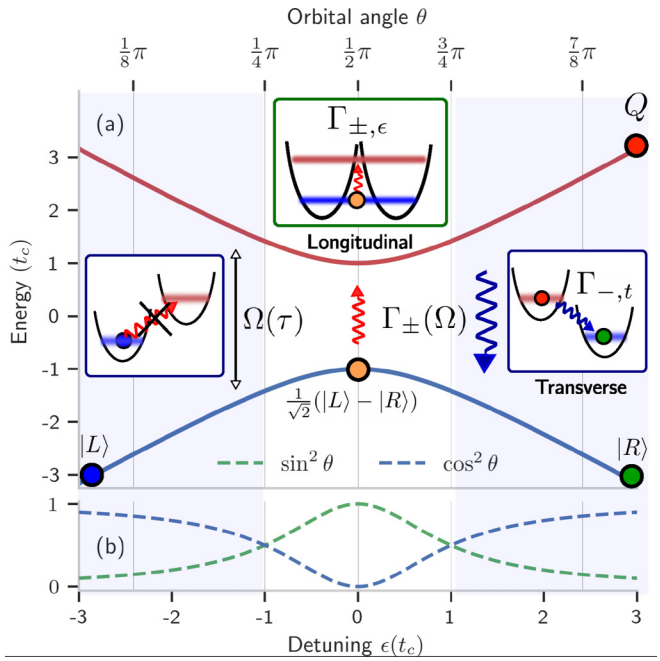

FIG. 1. A schematic picture of adiabatic transition between two quantum dots in presence of charge noise and phonon bath. In panel (a), we show energy of instantaneous states $|\pm,\theta\rangle$ (red/blue lines) as a function of detuning ϵ (lower axis) and orbital angle $\theta = \mathrm{arccot}(-\epsilon/t_c)$ (upper axis). Despite detuning sweep being adiabatic ($t_c^2 \gg v$), the electron initialized in the left dot (blue circle) can still end up with nonzero occupation of excited state localized in right dot Q (red circle) as a result of coupling to environment, which leads to incoherent transitions, between eigenstates of the instantaneous Hamiltonian, characterized by the rates $\Gamma_\pm(\Omega)$. At low temperatures, the excitation rate is non-negligible only in vicinity of avoided crossing, where the gap is smallest, $\Omega(0) = t_c$, while relaxation accounts for recovery of ground state occupation (the "healing" of the excitation) at larger detuning. As the detuning is changed, the character of eigenstates of the instantaneous Hamiltonian, $|\pm,\theta\rangle$, is modified from dotlike character at $|\epsilon| \gg t_c$ to orbital-molecular-like at $|\epsilon| \ll t_c$, which is accompanied by dominant role of transverse (interdot) and longitudinal transitions, respectively, see Sec. III A. To illustrate the difference between them, in panel (b), we plot $\cos^2\theta = |\langle +,\theta|\sigma_z|+,\theta\rangle|^2$ (dashed blue) and $\sin^2\theta = |\langle +,\theta|\sigma_x|+,\theta\rangle|^2$ (dashed green) factor that determine the relative importance of transverse Γ_t and longitudinal Γ_ϵ relaxation channels, respectively. Insets with green and blue frames schematically representing transition mechanisms dominant in regimes of $\epsilon \ll -t_c$, $|\epsilon| \ll t_c$, and $\epsilon \gg t_c$.

We assume the electron is initialized in the ground state at large negative detuning $\epsilon(-\tau_\infty) \ll t_c$, such that the initial state $|\psi(-\tau_\infty)\rangle = |-,\theta(-\tau_\infty)\rangle \approx |L\rangle$. Due to non-negligible coupling between the adiabatic states during the system's evolution (i.e., a nonzero $\dot\theta(\tau)$ term in Eq. (6)), a nonzero occupation of excited state $|+,\theta(\tau)\rangle$ can be generated. When the detuning sweep terminates at large $\epsilon(\tau_\infty) \gg t_c$, the occupation of excited state defines the transfer error, i.e., the probability of the electron being left behind in the L dot:

$$Q = |\langle\psi(\tau_\infty)||+,\theta(\tau_\infty)\rangle|^2 \approx |\langle\psi(\tau_\infty)|L\rangle|^2. \tag{8}$$

The calculation of Q for an electron coupled to environments relevant for semiconductor-based gated QDs is the main goal of this paper.

For constant tunnel coupling t_c and for $\epsilon(\tau) = v\tau$, we are dealing with the well-known LZ model [28], in which Q is given by Q_{LZ} from Eq. (2). We concentrate here on the adiabatic regime, defined by $Q_{\mathrm{LZ}} \ll 1$, which implies $t_c^2/v \gg 1$, and means that the ratio of transverse and longitudinal terms in the effective Hamiltonian, Eq. (6), fulfills

$$\frac{\dot\theta}{\Omega} = \frac{v t_c}{\Omega^3} < \frac{v}{t_c^2} \ll 1\,. \tag{9}$$

This is the adiabatic condition for the dynamics of a closed and noise-free system. When it is fulfilled during detuning sweep, the electron remains at all times in the ground state $|-,\theta(\tau)\rangle$, which means it physically moves from the state initially localized in the left dot $|-,\theta(-\tau_\infty)\rangle = |L\rangle$, to a final state $|-,\theta(\tau_\infty))\rangle = |R\rangle$, located in the right dot.

B. Dynamics of an open system

We use here the AME approach [50,52,55,66], in which transitions caused by the environment occur between the instantaneous eigenstates of $\hat H(\tau)$, which are given by Eqs. (3). Our focus on the adiabatic regime ($t_c^2 \gg v$), combined with relatively weak coupling to charge noise (with noise rms $\sigma \ll t_c$) and short intrinsic correlation time of phonon bath allow us to use here a Lindbladian form of AME [41,42], which reads

$$\partial_\tau \hat\varrho_A = i[\hat{\mathcal{H}}(\tau), \hat\varrho_A] + \Gamma_+(\tau)\mathcal{D}[\hat\varsigma_+]\hat\varrho_A + \Gamma_-(\tau)\mathcal{D}[\hat\varsigma_-]\hat\varrho_A, \tag{10}$$

where $\hat\varrho_A = \hat U(\theta)\hat\varrho_{\mathrm{LR}}\hat U^\dagger(\theta)$ and ϱ_{LR} is the density matrix of the system before switching the description to the "adiabatic" frame, $\hat\varsigma_+ = |+,\theta\rangle\langle -,\theta|$, $\hat\varsigma_- = |-,\theta\rangle\langle +,\theta|$, and

$$\mathcal{D}[\hat o]\hat\varrho = \hat o\hat\varrho o^\dagger - \tfrac{1}{2}\{\hat o^\dagger\hat o, \hat\varrho\} \tag{11}$$

is the Lindbladian associated with operator $\hat o$ and time-dependent relaxation/excitation rate $\Gamma_\pm(\tau)$. In this approach, these rates depend on time though their dependence on the value of instantaneous energy splitting $\Omega(\tau)$ from Eq. (7), i.e., $\Gamma_\pm(\tau) = \Gamma_\pm[\Omega(\tau)]$. Below we will use both notations, $\Gamma_\pm(\tau)$ and $\Gamma_\pm[\Omega(\tau)]$, depending on context. In particular, if noise-induced excitations dominate over the LZ effect due to deterministic time dependence of $\hat H(\tau)$, i.e., $Q_{\mathrm{noise}} \gg Q_{\mathrm{LZ}}$, the unitary evolution can be safely neglected and Eq. (10) reduces to a simple rate equation

$$\dot Q(\tau) \approx \Gamma_+(\tau) - Q(\tau)(\Gamma_-(\tau) + \Gamma_+(\tau)), \tag{12}$$

where $Q(\tau) = \langle +,\theta|\hat\varrho_A(\tau)|+,\theta\rangle$ denotes occupation of the higher energy state $|+,\theta\rangle$ at time τ.

Given the initial condition $Q(-\tau_\infty) = 0$, the solution to Eq. (12) reads

$$\begin{aligned} Q &= \int_{-\tau_\infty}^{\tau_\infty} d\tau\, \Gamma_+(\tau) e^{-\int_\tau^{\tau_\infty} \Gamma_+(\tau')+\Gamma_-(\tau')d\tau'} \\ &= \int_{-\tau_\infty}^{\tau_\infty} d\tau \Gamma_+(\tau) e^{-\chi(\tau,\tau_\infty)}, \end{aligned} \tag{13}$$

where

$$\chi(\tau,\tau_\infty) = \int_\tau^{\tau_\infty} (\Gamma_+ + \Gamma_-)d\tau'\,. \tag{14}$$

C. Approximate solutions

Let us now discuss a few physically motivated approximate solutions for the probability of ending up in the excited state at the end of the sweep Q, i.e., the probability that the electron remains in the initial dot. We start with a simplest perturbative approach to rate Eq. (12), assuming $\Gamma_{\pm}\tau_{\infty} \ll 1$. In the lowest order, one can write

$$Q^{(1)} = \int_{-\tau_{\infty}}^{\tau_{\infty}} \Gamma_{+}(\tau) d\tau. \tag{15}$$

As the energy needed for transition from the ground to excited state comes from thermal fluctuations of environment, the excitation rate Γ_{+} is strongly suppressed at low temperatures, when $k_B T \ll t_c \leqslant \Omega(\tau)$. At these temperatures the rate of energy relaxation into the environment, $\Gamma_{-}(\Omega)$, is temperature independent, as the thermal occupation factor for environmental states of energy $\Omega \gg k_B T$ is zero, and $\Gamma_{-}(\Omega)$ depends then only on density of environmental states and coupling matrix elements. For all the environments considered in this paper, these dependencies lead to a power-law behavior of the rates, $\Gamma_{-}(\Omega) \propto \Omega^{a}$ with $a \in [-3, 3]$, depending on the transition mechanism and range of Ω, see derivations in the next section. As we assume the environment to be in thermal equilibrium, the detailed balance condition, which reads $\Gamma_{+}(\Omega) = \Gamma_{-}(\Omega) e^{-\beta\Omega}$, leads to $\Gamma_{+}(\Omega) \propto \Omega^{a} e^{-\beta\Omega}$ with $e^{-\beta\Omega} \ll 1$ at low temperatures.

The excitation process then takes place in a narrow range of detunings around the avoided crossing, as $\Gamma_{+}(\Omega)$ very quickly decreases when $|\epsilon|$ increases. As $\beta\Omega(\tau) \approx \beta t_c + \beta v^2 \tau^2 / 2t_c$ for $\epsilon \ll t_c$, we neglect in this regime the ϵ dependence of $\Gamma_{+}(\Omega)$ and replace it with value for $\Omega = t_c$ (equivalently, for $\tau = 0$), while we keep it in the thermal factor. The integrand in Eq. (15) can then be approximated as $\Gamma_{+}(\tau) \approx \Gamma_{-}(0) e^{-\beta\Omega(\tau)}$, and the integration can be done over a range of $|\epsilon| \ll t_c$. In this way, we obtain the single excitation approximation limit (SEAL),

$$\begin{aligned} Q_{\mathrm{SEAL}} &= \Gamma_{-}(0) e^{-\beta t_c} \int_{-\infty}^{\infty} e^{-\frac{\beta v^2 t^2}{2t_c}} d\tau \,, \\ &= \frac{\sqrt{2\pi k_{\mathrm{B}} T t_c}}{v} \Gamma_{-}(0) e^{-\beta t_c} \,, \end{aligned} \tag{16}$$

which assumes that, at most, a single quantum jump from ground to excited state takes place in the avoided crossing region. We highlight that contrary to coherent nonadiabatic transitions (LZ), the occupation of the excited state caused by the energy absorption at avoided crossing increases as the sweep rate gets smaller, i.e., $Q_{\mathrm{SEAL}} \propto 1/v$. It is a direct consequence of the electron spending more time at vicinity of avoided crossing, where transition from ground to excited state is exponentially more probable.

The SEAL approximation does not take into account the possibility of an electron transition in the opposite direction, i.e., from excited to ground state, which would lead to partial recovery of ground-state occupation—an effect that we will refer to as a healing of excitation that occurred close to the anticrossing. This effect is captured by the $\exp[-\chi(\tau)]$ factor in Eq. (13) with $\chi(\tau)$, given in Eq. (14)), evaluated in the low-temperature limit of $\Gamma_{-} \gg \Gamma_{+}$. The effect of transitions occurring during the part of the sweep when $\epsilon(\tau) > t_c$ is captured by a *healed excitation approximation limit* (HEAL):

$$Q_{\mathrm{HEAL}} \approx Q_{\mathrm{SEAL}} \exp\left(- \int_{0}^{\tau_{\infty}} \Gamma_{-}(\tau) \, d\tau \right). \tag{17}$$

The physical picture expected to hold at low T is thus the following. A finite Q is generated due to coupling to a thermal reservoir near the anticrossing, and then processes of emission of energy into this reservoir lead to a diminishing of its final value at the end of the sweep, making the final state of the system closer to the one following from an ideal adiabtic evolution. Such a healing process results in environment-assisted inelastic tunneling into the ground state at the end of the driving, see Fig. 1. In Sec. IV, we will demonstrate in which regimes of parameters the SEAL/HEAL solutions are applicable for realistic double quantum dot (DQD) devices.

Note that up to this moment we have not specified any particular form of relaxation/excitation rates $\Gamma_{\pm}(\tau)$, which makes the above approximations also suitable for other systems described in terms of the LZ Hamiltonian Eq. (1) in the adiabatic limit ($t_c^2 \gg v$) and coupled to environment at relatively low temperature ($t_c \gtrsim k_{\mathrm{B}} T$).

III. TRANSITION RATES FOR AN ADIABATICALLY TRANSFERRED ELECTRON

A. General properties

We consider now a transfer of an electron between two QDs that is driven by a detuning sweep slow enough to be adiabatic in the closed system limit. After turning on a weak coupling to an environment, the transition rates $\Gamma_{\pm}(\tau)$ in the AME from Eq. (10) are evaluated at given τ as if the system described by the instantaneous Hamiltonian $\hat{H}(\tau)$ from Eq. (1) was subjected to an off-diagonal coupling with an environment for a long enough time for Fermi's golden rule (FGR) calculation to be applicable. Thus the general form of electron-environment coupling $\hat{V} = \frac{1}{2}(\hat{V}_t \hat{\sigma}_x + \hat{V}_\epsilon \hat{\sigma}_z)$ in the $|L/R\rangle$ basis at given $\theta(\tau)$ should be expressed in the basis of eigenstates of instantaneous Hamiltonian, $|\pm, \theta\rangle$, using $\hat{\mathcal{V}}(\theta) = \hat{U}_y^{\dagger}(\theta) \hat{V} \hat{U}_y(\theta)$, which leads to

$$\hat{\mathcal{V}}(\theta) = \tfrac{1}{2}(\hat{\mathcal{V}}_x \hat{\varsigma}_x + \hat{\mathcal{V}}_z \hat{\varsigma}_z), \tag{18}$$

where $\hat{\mathcal{V}}_x = (\hat{V}_t \cos\theta + \hat{V}_\epsilon \sin\theta)$ and $\hat{\mathcal{V}}_z = (\hat{V}_\epsilon \cos\theta - \hat{V}_t \sin\theta)$. This means that at every τ we do the FGR calculation for $\hat{\mathcal{V}}_x \hat{\varsigma}_x / 2$ coupling, where $\hat{\varsigma}_x$ acts in basis of eigenstates of the instantaneous $\hat{H}(\tau)$. With the environmental Hamiltonian given by $\hat{H}_E$, we then calculate the quantum spectral density for the operator $\hat{\mathcal{V}}_x(t) = e^{i\hat{H}_E t} \hat{\mathcal{V}}_x e^{-i\hat{H}_E t}$, given by [69,72]

$$S_{\mathcal{V}}^{Q}(\omega) = \int_{-\infty}^{\infty} \langle \hat{\mathcal{V}}_x(t) \hat{\mathcal{V}}_x(0) \rangle e^{i\omega t} dt, \tag{19}$$

where $\langle \ldots \rangle = \mathrm{Tr}_E(\hat{\rho}_E \ldots)$ is the averaging over the environmental density matrix $\hat{\rho}_E$. The rate of excitation of the system, i.e., a transition that involves taking energy $\Omega(\tau)$ from the environment, is then given by [69,72]

$$\Gamma_{+}(\tau) = \tfrac{1}{4} S_{\mathcal{V}}^{Q}[-\Omega(\tau)], \tag{20}$$

while the relaxation rate is

$$\Gamma_{-}(\tau) = \tfrac{1}{4} S_{\mathcal{V}}^{Q}[\Omega(\tau)]. \tag{21}$$

For an environment in thermal equilibrium which we consider here, we have $\hat{\rho}_E \propto e^{-\beta \hat{H}_E}$ and the detailed balance condition, $S_V^Q(\Omega) = S_V^Q(-\Omega)e^{\beta\Omega}$, and thus $\Gamma_-[\Omega(\tau)] = \Gamma_+[\Omega(\tau)]e^{\beta\Omega(\tau)}$, is fulfilled.

As the longitudinal $\hat{V}_\epsilon$ and transverse $\hat{V}_t$ couplings in dot basis are often of different physical origin, we assume $\langle \hat{V}_\epsilon \hat{V}_t \rangle = 0$, so the transition rate can be written as $\Gamma_\pm(\tau) = \Gamma_{\epsilon,\pm}(\tau) + \Gamma_{t,\pm}(\tau)$, where we introduced

$$\text{(Longitudinal)}: \quad \Gamma_{\epsilon,\pm}(\tau) = \tfrac{1}{4}\sin^2\theta \; S_\epsilon^Q[\mp\Omega(\tau)],$$
$$\text{(Transverse)}: \quad \Gamma_{t,\pm}(\tau) = \tfrac{1}{4}\cos^2\theta \; S_t^Q[\mp\Omega(\tau)] \qquad (22)$$

contributions, defined using spectral densities of $\hat{V}_\epsilon$ and $\hat{V}_t$ operators, $S_\epsilon^Q(\omega) = \int \langle \hat{V}_\epsilon(t)\hat{V}_\epsilon(0)\rangle e^{i\omega t} dt$ and $S_t^Q(\omega) = \int \langle V_t(t)\hat{V}_t(0)\rangle e^{i\omega t} dt$. The $\hat{V}_\epsilon \hat{\sigma}_z$ coupling that is longitudinal in the $|L/R\rangle$ basis (the dot basis) appears due to fluctuations of detuning or phonons coupling to the operator $\hat{\sigma}_z$. It is most efficient at causing transitions between $|\pm,\theta\rangle$ states when the latter have a molecular-orbital character, i.e., $\theta \approx \pi/2$, $\sin^2\theta \approx 1$, $|\pm,\pi/2\rangle = \frac{1}{2}(|L\rangle \pm |R\rangle)$, and $|\epsilon| \ll t_c$. On the other hand, the transverse coupling $\hat{V}_t\hat{\sigma}_x$ is due to fluctuations of tunnel coupling or phonons coupling to the operator $\hat{\sigma}_x$. It leads to transitions of interdot character between the states $|L\rangle \leftrightarrow |R\rangle$ that correspond to $|\pm,\theta\rangle$ states at $\theta \ll 1$ and $\theta \approx \pi$ (i.e., $\epsilon \ll -t_c$ and $\epsilon \gg t_c$, respectively), see Fig. 7(b). Below we will see that for all considered mechanisms, the transverse processes are weaker than the longitudinal ones, i.e., $S_t^Q(\Omega) \ll S_\epsilon^Q(\Omega)$, so the latter could become relevant only in a very far-detuned regime.

For an electron in a double QD, the relevant mechanisms of transitions between the eigenstates are due to coupling of electron charge to two reservoirs: lattice vibrations (phonons) and sources of fluctuations of electric fields—free electrons in metallic electrodes and ungated regions of semiconductor quantum wells being the sources of Johnson noise, and bound charges switching between a discrete number of states being the sources of $1/f$ type noise [73]. Due to their distinct physical origin, we neglect correlations between different transition mechanisms and write the relaxation rate as

$$\Gamma_- = \Gamma_-^{(\mathrm{ph})} + \Gamma_-^{(1/f)} + \Gamma_-^{(\mathrm{Joh})}. \qquad (23)$$

In the above, we separated charge noise contribution into $\Gamma^{(1/\mathrm{f})}$ due to tail of $1/f$-like noise from TLFs [65] in the quantum well interface and $\Gamma^{(\mathrm{Joh})}$ due to Johnson's noise caused by wiring in the vicinity of QDs [74]. As a direct consequence of Eq. (23), the exact formula for leaving electrons in the initial dot reads

$$Q = \int_{-\tau_\infty}^{\tau_\infty} d\tau \sum_m \Gamma_+^{(m)}(\tau) \exp\left(-\sum_{m'} \chi^{(m')}(\tau, \tau_\infty)\right), \qquad (24)$$

where indices m, m' stand for phonon, $1/f$, or Johnson's mechanisms, while $\chi^{(m)}(a,b) = \int_a^b \Gamma_+^{(m)}(\tau') + \Gamma_-^{(m)}(\tau')d\tau'$.

Let us now discuss the quantum noise spectra relevant for the two types of reservoirs being the sources of charge noise and the lattice vibrations.

B. Charge noise

The way in which sources of charge noise couple to the electron in a DQD is most easily visible if we consider the high-temperature (or low energy transfer) limit of $\beta\Omega \ll 1$. The quantum spectral density then becomes symmetric in frequency, $S_V^Q(\Omega) = S_V^Q(-\Omega)$ (so $\Gamma_+ = \Gamma_-$), and it can be identified with a classical power spectral density of a classical stochastic process describing the fluctuations of the electric fields caused by the dynamics of the reservoir. These processes manifest themselves as time-dependent corrections to parameters of $\hat{\mathcal{H}}(\tau)$: $\delta\epsilon(\tau)$ and $\delta t(\tau)$ for detuning and tunnel coupling noise, respectively. As long as the amplitude of the noise is small ($\delta t, \delta\epsilon \ll t_c$), the modification of the instantaneous splitting $\Omega(\tau) = \sqrt{(v\tau + \delta\epsilon)^2 + (t_c + \delta t)^2}$ is negligible. However, time variation of $\delta\epsilon$ and δt activates coupling between the eigenstates of the instantaneous Hamiltonian from Eq. (6)), as in the lowest order in $\delta\epsilon$ and δt we have

$$\dot{\theta} = \frac{\partial}{\partial\tau}\mathrm{acot}\left(-\frac{v\tau + \delta\epsilon}{t_c + \delta t}\right) \approx \frac{\sin\theta\,\delta\dot{\epsilon} + \cos\theta\,\delta\dot{t}}{\Omega_0}, \qquad (25)$$

where $\Omega_0 = \sqrt{v^2\tau^2 + t_c^2}$ and the last approximation relies on $t_c^2 \gg v$ assumption to neglect contributions not larger than the noiseless coupling $\dot{\theta}_0 = vt_c/\Omega_0^2 \ll \Omega$, see Eq. (9). As we neglect correlations between $\delta\epsilon$ and δt, we treat the transitions induced by these two noises independently. Then taking into account that the classical spectrum $S_{\dot{x}}^{cl}(\omega) = \int \langle \dot{x}(t)\dot{x}(0)\rangle e^{i\omega t} dt$ (where $\langle \ldots \rangle$ now denotes averaging over realizations of noise) is related to the classical spectrum of $x(t)$ noise by $S_{\dot{x}}^{cl}(\omega) = \omega^2 S_x^{cl}(\omega)$, and that $\sin^2\theta = t_c^2/\Omega_0^2$ and $\cos^2\theta = (v\tau)^2/\omega_0^2$, we have

$$\Gamma_{\pm,\epsilon}(\tau) = \frac{1}{4}\frac{t_c^2}{\Omega_0^2(\tau)} S_\epsilon^{cl}[\mp\Omega_0(\tau)], \qquad (26)$$

$$\Gamma_{\pm,t}(\tau) = \frac{1}{4}\frac{(v\tau)^2}{\Omega_0^2(\tau)} S_t^{cl}[\mp\Omega_0(\tau)]. \qquad (27)$$

In these equations, the $\mp\Omega_0$ arguments can be, of course, replaced by $|\Omega_0|$, as the classical spectra are symmetric in frequency. In Appendix A, we give an alternative derivation of these results (in the spirit of methods used previously in Refs. [38,61]). We also show there that the AME calculation using these rates agrees very well with direct averaging of evolution due to $\hat{H}(\tau)$ averaged over realizations of classical noise with experimentally relevant parameters (discussed below in this section). In this way, we check the applicability of AME to the system of interest in this paper in the classical noise/high-temperature regime.

Equations (26) and (27) connect the rates as given τ with (classical) spectra of appropriate noise at $\pm\Omega_0$ frequencies. Extension of AME to a regime of lower temperatures/higher Ω_0 then amounts to replacing the classical spectra, $S^{\mathrm{cl}}(\pm\Omega_0)$, by their quantum counterparts, $S^Q(\pm\Omega_0)$. Let us now discuss the classical and quantum regimes for the two charge noise spectra relevant for semiconductor QDs in GHz range ($t_c \sim 10\ \mu$eV) of energies.

First, we consider electric fluctuations from electron gas in metallic gates, the Johnson-Nyquist noise of general form [69,75,76]

$$S_\epsilon^{Q,(J)}(\omega) = \frac{\Re Z}{R_q}\frac{\omega}{1 - e^{-\beta\omega}}, \qquad (28)$$

where R_q is the inverse of conductance quantum $R_q = \pi/e^2 = 13\ \mathrm{k}\Omega$ and Z is the impedance of a noise source, which we model here as an ideal resistor (R) of the impedance given typically for microwaves $Z_R = R = 50\,\Omega$. The temperature-dependent part of Eq. (28) reduces to Bose-Einstein distribution $n(\omega) = 1/(e^{\beta\omega} - 1)$ for negative frequencies $\omega < 0$ (absorption) and $n(\omega) + 1$ for $\omega > 0$ (stimulated and spontaneous emission). In the $\gtrsim$ GHz frequency range relevant here, Johnson noise from a lossy transmission line discussed in Ref. [77] for Si/SiGe QD gives at most an order of magnitude larger noise power.

Next, we consider $1/f$-type fluctuations of electric field due to TLFs localized in the insulating regions of the nanostructure [73]. We focus first on noise in detuning, as there are numerous measurements of spectrum of this noise in DQDs. Due to very high spectral weight at low frequencies, such a $1/f$ noise dominates the dephasing of qubits, the energy splitting of which depends on electric fields [73,78]. Here, however, we focus on high (GHz range) positive and negative frequency behavior of $S^{Q,(1/f)}(\omega)$, that is, of $1/|\omega|^{\alpha}$ character at very low frequencies. The behavior of quantum noise caused by an ensemble of TLFs at such frequencies depends on the microscopic details of these fluctuators and the distribution of their parameters, see Ref. [65] and references therein.

Here, as in Ref. [79], where Si/SiGe charge qubit in a DQD was considered, we take $\alpha = 1$ with noise amplitude directly extrapolated from the low-frequency regime, i.e., for the positive-frequency quantum spectrum, we have

$$S_{\epsilon}^{Q,(1/f)}(\omega > 0) = s_1(T)\frac{\omega_1}{\omega}, \tag{29}$$

where $\omega_1 = 2\pi/\mathrm{s}$ and $s_1(T) = S^{cl}(\omega_1)$ is a commonly reported classical spectral density at $f = 1\,\mathrm{Hz}$, which at electron temperature of $T = 100\,\mathrm{mK}$ in a typical Si/SiGe device is given by $s_1(100\,\mathrm{mK}) \approx (0.3-2)^2\,\mu\mathrm{eV}^2/\mathrm{Hz}$ [80–84]. As $s_1(T) \propto T$ scaling was observed in experiments on QDs [82–84], we assume here $s_1(T) = s_1(100\,\mathrm{mK})\frac{T}{100\,\mathrm{mK}}$. The negative-frequency quantum spectrum follows from Eq. (29), using the detailed balance condition. It is commonly believed that charge disorder in SiMOS should have larger amplitude, for example, $s_1(100\,\mathrm{mK}) \approx 10\,\mu\mathrm{eV}^2/\mathrm{Hz}$ was measured in Ref. [85] at $T = 300\,\mathrm{mK}$. However, following Ref. [86] and references therein, we assume that the $1/f$ noise amplitude in SiMOS can be made comparable or even smaller than in Si/SiGe [82].

Let us stress that the character of noise generated by an ensemble of TLFs above $\sim$ MHz frequency is not universal, as its amplitude and exponent varies between DQD materials and devices. In particular, recent measurements of charge noise in Si/SiGe [87] and SiMOS [88] showed $1/f$ and $1/f^{0.7}$ scaling up to 100 MHz and 1 MHz, respectively, which contrasted with a few orders of magnitude weaker amplitude of charge noise at MHz frequencies in some GaAs singlet-triplet qubits [89,90]. Additionally, in neither experiment was a linear scaling of spectral density with temperature seen at highest frequencies, and, in particular, the Si/SiGe case showed only weak dependence on the temperature, confirmed also elsewhere for SiMOS [86,91], which stood in contrast to GaAs device, where $S(\omega) \propto T^2$ and the spectrum became flat, i.e., $\alpha \to 0$ as T was increased [89]. A recent theoretical study [65] of qubit relaxation caused by interaction with an ensemble of TLFs coupled to a thermal bath (which creates $1/f$ noise at low frequencies) showed that at high positive frequencies (between MHz and GHz, depending on temperature), a crossover first to $S^Q(\omega) \propto 1/\omega^2$ and then to a flat or Ohmic spectrum (depending on details of distribution of energies of the TLFs) occurs. One can thus expect that in measurement of high-frequency quantum noise, it is difficult to distinguish the noise caused by TLFs from other sources of electric field fluctuations, as a flat spectrum has already been observed at MHz frequency in SiMOS QD spectroscopy [92]. Let us note that one of the models of distribution of energies of TLFs considered in Ref. [65] led to $S^Q(\omega > 0) \propto T$ at high frequencies. In light of the above discussion, we use the above model to estimate the relevance of the tail of $1/f$ noise in silicon-based devices and set $s_1(0.1\mathrm{K}) = 1^2\,\mu\mathrm{eV}^2/\mathrm{Hz}$. We will use the same spectrum for GaAs, probably overestimating the noise in this case, but below we will show that for GaAs QDs the influence of electron-phonon coupling dominates over that of charge noise, even having such a large amplitude.

For the charge noise in tunnel coupling, we treat it is as uncorrelated with the noise in detuning. While considerations of microscopic noise models (e.g., of $1/f$ noise caused by an ensemble of TLF's localized in the vicinity of the DQD [93]) clearly show that the two noises should be expected to be correlated to some degree—in a detailed derivation of transition rates in Appendix A, we show that in the leading order of perturbation theory, the rates due to noise in ϵ and t_c appear to follow from uncorrelated noises, unless their correlations are of causal nature. The latter means that $\langle\delta\epsilon(\tau)\delta t(0)\rangle - \langle\delta t(\tau)\delta\epsilon(0)\rangle \neq 0$, which can arise, for example, when one takes into account interactions between the TLFs in modeling $1/f$ noise [94]. The significance of such correlations has not yet been explored for charge noise affecting QDs, and we choose to neglect it here.

We parametrize the ratio of rms of fluctuations of the noise in t_c and ϵ by $\eta = \sqrt{S_t(\omega)/S_\epsilon(\omega)} \approx 0.1$, with its value motivated by semiconductor QD experiments [25,87,89,95], and typical values of the lever arm used to control the electronic gates during shuttling [24]. We conclude this section by giving the explicit forms of longitudinal and transverse contributions to relaxation rates due to charge noise,

$$\Gamma_{-,\epsilon}(\tau) = \frac{1}{4}\left(\frac{t_c}{\Omega(\tau)}\right)^2 S_{\epsilon}^{Q}[\Omega_0(\tau)]\,, \tag{30}$$

$$\Gamma_{-,t}(\tau) = \frac{\eta^2}{4}\left(\frac{v\tau}{\Omega(\tau)}\right)^2 S_{\epsilon}^{Q}[\Omega_0(\tau)]\,, \tag{31}$$

which are applicable for both $1/f$ and Johnson noise. The corresponding excitation rates are obtained via detailed balance condition $\Gamma_+(\Omega) = \Gamma_-(\Omega)e^{-\beta\Omega}$.

C. Electron-phonon interaction

In semiconductors, another mechanism responsible for transitions between the $|\pm,\theta\rangle$ states is associated with energy exchange between the electron and lattice vibrations. Phonons are assumed to be in thermal equilibrium, with their free Hamiltonian given by $H_{\mathrm{ph}} = \sum_{\mathbf{k},\lambda}\omega_{\mathbf{k},\lambda}b^{\dagger}_{\mathbf{k},\lambda}b_{\mathbf{k},\lambda}$, where λ and

k represents phonon polarizations and wave vector, respectively. The electron-phonon interaction is given by [96]

$$\mathcal{H}_{\text{el-ph}} = \sum_{j,\mathbf{k},\lambda=L,T} \sqrt{\frac{|\mathbf{k}|}{2\varrho c_\lambda V}}\, v^{(j)}_{\mathbf{k},\lambda}(\hat{b}_{\mathbf{k},\lambda} + \hat{b}^\dagger_{-\mathbf{k},\lambda}) e^{i\mathbf{kr}}, \quad (32)$$

in which ϱ denotes crystal density, V the crystal volume, and c_λ is the speed of λ-polarized phonons. The coupling $v^{(j)}_{\mathbf{k},\lambda}$ stands for piezoelectric ($j = p$) and deformation potential ($j = d$), evaluated for transverse ($\lambda = T$) and longitudinal ($\lambda = L$) polarizations of phonons,

$$v^{(\mathrm{p})}_{\mathbf{k},\lambda} = \frac{\chi_p}{k}, \quad v^{(d)}_{\mathbf{k},L} = \Xi_d + \Xi_u \left(\frac{k_z}{k}\right)^2, \quad v^{(d)}_{\mathbf{k},T} = -\Xi_u \frac{k_{xy} k_z}{k^2}, \quad (33)$$

where χ_p is piezoelectric constant, while Ξ_d, Ξ_u are dilatation and shear deformation potentials, respectively. In GaAs and Si, the coupling to phonons takes a very different form, namely, Si lacks the dominant in the GaAs piezoelectric coupling $\chi_p^{\mathrm{SiGe}} = 0$ [97], while the opposite is true for shear deformation potential since $\Xi_u^{\mathrm{GaAs}} = 0$.

We evaluate the matrix elements of interaction from Eq. (32) in the two-dimensional space spanned by $|L/R\rangle$ states (see Appendix B for details), obtain the $\hat{V}_t\hat{\sigma}_x + \hat{V}_\epsilon\hat{\sigma}_z$ form of coupling discussed in Sec. III A, and arrive at quantum spectra associated with longitudinal ($\hat{V}_\epsilon$) and transverse ($\hat{V}_t$) couplings to phonons:

$$S^{(\mathrm{ph})}_{\epsilon/t}[\Omega(\tau)] = 4\pi \sum_{j,\mathbf{k},\lambda} \frac{k\left|v^{(j)}_{\mathbf{k},\lambda}\right|^2}{\varrho c_\lambda V} |\mathcal{M}_{\epsilon/t}(\mathbf{k})|^2 \frac{\delta(\Omega(\tau) - \omega_{\mathbf{k},\lambda})}{1 - e^{-\beta\omega_{\mathbf{k},\lambda}}}, \quad (34)$$

where the matrix elements read $\mathcal{M}_\epsilon(\mathbf{k}) = \langle L|e^{i\mathbf{kr}}|L\rangle - \langle R|e^{i\mathbf{kr}}|R\rangle$ and $\mathcal{M}_t(\mathbf{k}) = \langle L|e^{i\mathbf{kr}}|R\rangle + \langle R|e^{i\mathbf{kr}}|L\rangle$, while the temperature-dependent term reduces to Bose-Einstein distribution $n(\Omega)$ for $\Omega < 0$ (absorption) and to $n(\omega) + 1$ for $\Omega > 0$ (emission). The transition rates are given by

$$\Gamma^{(\mathrm{ph})}_{\pm,\epsilon}(\tau) = \tfrac{1}{4}\sin^2\theta\, S^{(\mathrm{ph})}_\epsilon[\mp\Omega(\tau)], \quad (35)$$

$$\Gamma^{(\mathrm{ph})}_{\pm,t}(\tau) = \tfrac{1}{4}\cos^2\theta\, S^{(\mathrm{ph})}_t[\mp\Omega(\tau)]. \quad (36)$$

For further calculation, we need to specify a model of $\langle \mathbf{r}|L_0/R_0\rangle$ wave functions localized in the uncoupled dots. We assume that they are separable and Gaussian:

$$\langle \mathbf{r}|L_0/R_0\rangle = \frac{1}{\left(\pi^3 r_{xy}^4 r_z^2\right)^{\frac{1}{4}}} \exp\left(-\frac{\left(x \mp \frac{\Delta x}{2}\right)^2 + y^2}{2r_{xy}^2} - \frac{z^2}{2r_z^2}\right), \quad (37)$$

where the full width at half maximum (FWHM) of the electron wave function, which defines the *dots diameter*, is given by $2r_{xy}$ in planar and $2r_z$ in the growth direction of structure, while the Δx gives the distance between the dots. Next we use the Hund-Mulliken approximation [98,99] to generate a set of orthogonal states in DQD systems that fulfill $\langle L|R\rangle = 0$, which can be done by setting:

$$|L/R\rangle = |L_0/R_0\rangle - g|R_0/L_0\rangle, \quad (38)$$

where $g \approx \frac{1}{2}\langle L_0|R_0\rangle = \frac{1}{2}e^{-\Delta x^2/4r_{xy}^2} \ll 1$.

As the energy quanta exchanged between the electron and the lattice are < 1 meV, we take into account only the acoustic phonons with $\omega_{\mathbf{k},\lambda} = c_\lambda|\mathbf{k}|$. The relaxation rates due to electron-phonon interaction are then given by

$$\Gamma^{(\mathrm{ph})}_{-,\epsilon}(\Omega) = \sum_{\lambda,j} \frac{\Omega t_c^2}{8\pi^2\varrho c_\lambda^5} \int d\Omega_{\mathbf{k}} \left|v^{(j)}_{\mathbf{k}_\lambda,\lambda}\right|^2 |F_\epsilon(\mathbf{k}_\lambda)|^2 [n(\Omega) + 1], \quad (39)$$

$$\Gamma^{(\mathrm{ph})}_{-,t}(\Omega) = \sum_{\lambda,j} \frac{\Omega\,\epsilon^2}{8\pi^2\varrho c_\lambda^5} |\langle L_0|R_0\rangle|^2 \int d\Omega_{\mathbf{k}} \left|v^{(j)}_{\mathbf{k}_\lambda,\lambda}\right|^2 |F_t(\mathbf{k}_\lambda)|^2 \times [n(\Omega) + 1], \quad (40)$$

where the integration over the solid angle of resonant wave vector $\mathbf{k}_\lambda$, with length $k_\lambda = \Omega/c_\lambda$ was denoted by $d\Omega_{\mathbf{k}} = d\vartheta_{\mathbf{k}} d\varphi_{\mathbf{k}} \sin\vartheta_{\mathbf{k}}$, while the form factors read

$$|F_t(\mathbf{k})|^2 = \exp\left(-\frac{k_{xy}^2 r_{xy}^2 + k_z^2 r_z^2}{2}\right)\left(1 - \cos\left(\tfrac{k_x \Delta x}{2}\right)\right)^2,$$
$$|F_\epsilon(\mathbf{k})|^2 = \exp\left(-\frac{k_{xy}^2 r_{xy}^2 + k_z^2 r_z^2}{2}\right)\sin^2\left(\tfrac{k_x \Delta x}{2}\right). \quad (41)$$

The common term $\exp(-(k_{xy}^2 r_{xy}^2 + k_z^2 r_z^2)/2)$ is the Fourier transform of the electron wave function, while the main difference between the longitudinal and transverse relaxation is the overlap of bare dots wave functions, $|\langle L_0|R_0\rangle|^2 = e^{-\Delta x^2/2r_{xy}^2} \ll 1$ which makes the transverse relaxation mechanism orders of magnitude weaker, i.e., $\Gamma^{(\mathrm{ph})}_{-,t} \ll \Gamma^{(\mathrm{ph})}_{-,\epsilon}$, unless detuning is so large that θ is close enough to π for the $\sin^2\theta$ term in Eq. (35) to suppress $\Gamma^{(\mathrm{ph})}_{-,\epsilon}$ to the degree that is becomes smaller than $\Gamma^{(\mathrm{ph})}_{-,t}$.

As the size of the QD in planar direction r_{xy} is larger then the size in the z direction, $2r_z \ll r_{xy}$, its value can be extracted from splitting between the ground and first excited dot state ΔE, i.e., $r_{xy} = \sqrt{1/m^*\Delta E}$. In Si at $\Delta E = 1$ meV, an estimate of $r_{xy} \approx 20$ nm is consistent with reported values of $r_{xy} \approx 15$ nm [100], 13 nm [81] in Si/SiGe and $r_{xy} \approx 21$ nm [101], 18 nm [85] in SiMOS. The GaAs dots are typically larger ($r_{xy} \approx 55$ nm [102], 21 nm [103]), mostly due to smaller effective mass, i.e., $m^*_{\mathrm{Si}}/m^*_{\mathrm{GaAs}} \approx 3$. The typically reported values of $2r_z \approx 20$ nm [102] in GaAs are also larger than those in Si/SiGe, $2r_z \approx 4$ nm [104], 6 nm [81]. We assume here the extent of electron's wave function in the z direction in SiMOS is similar to that in Si/SiGe, and for both we take it as $2r_z = 5$ nm. Finally, smaller dots allow for decreasing the distance between the sites typical for GaAs $\Delta x \approx 150$ nm [102], ≈110 nm [103] to Si/SiGe values of $\Delta x \approx 100$ nm [4] to SiMOS $\Delta x \approx 50$ nm [4]. The distances between the dots are correlated with reported values of t_c, the largest of which are achieved in SiMOS structures, with examples of $t_c \approx 450\,\mu$eV and 50 μeV for dots separated by $\Delta x \approx 40$ nm [27] and ≈100 nm [101], respectively. However, recently, $t_c \approx 40\,\mu$eV was achieved in Si/SiGe across an array of QDs with $r_{xy} \approx 10$ nm and $\Delta x \approx 70$ nm [24]. In GaAs, tunnel coupling of $t_c \approx 20 - 40\,\mu$eV was measured in an array of eight QDs with $\Delta x \approx 150$ nm [2] for an array of eight QDs. Representative parameters for each nanostructure that we will use in subsequent calculations are given in Table I.

We now evaluate numerical values of relaxation rates from Eqs. (39) and (40) for the above-discussed parameters of typical GaAs, Si/SiGe and SiMOS double QDs given in Table I,

TABLE I. Parameters used in the paper.

Quantity	Symbol	Values
Tunnel coupling	t_c	$5-60\,\mu$eV
Effective electron temperature	T	50−500 mK
Detuning sweep rate	v	$1-3000\,\mu$eV/ns
Initial detuning	ϵ_i	$-500\,\mu$eV
Final detuning	ϵ_f	$500\,\mu$eV
Time of detuning sweep	$\epsilon_f-\epsilon_i=\Delta\epsilon/v$	0.3−1000 ns
Transverse/longitudinal noise ratio	$\sqrt{S_t(\omega)/S_\epsilon(\omega)}$	0.1
Resistance of noisy resistor (Johnson noise)	Z_R	50Ω
$1/f$ noise amplitude at $T=0.1$ K	$s_1(0.1\,\mathrm{K})$	$1\,\mu\mathrm{eV}^2/\mathrm{Hz}$
Dots separation	Δx	150 nm (GaAs), 100 nm (SiGe), 50 nm (SiMOS)
Spread of electron wave function in XY plane	r_{xy}	40 nm (GaAs), 20 nm (Si/SiGe, SiMOS)
Width of quantum well	$2r_z$	20 nm (GaAs), 5 nm (Si/SiGe, SiMOS)

In Fig. 2, we plot zero-temperature electron relaxation rate due to scattering with phonons, $\Gamma_-^{(\mathrm{ph})}(\Omega)$, as a function of detuning ϵ (let us recall that $\Omega=\sqrt{t_c^2+\epsilon^2}$) for three values of tunnel coupling, $t_c=10, 20, 40\,\mu$eV. It is clear that the scattering of a single electron in a DQD in each of considered nanostructures is dominated by a different mechanisms. In polar GaAs, the piezoelectric coupling dominates over the deformation potential one, with the fastest relaxation at low detuning, where the transitions occur between molecular-orbital-type states. The relaxation rate, for the energies below $c/\Delta x\approx 50\,\mu eV$ shows oscillatory behavior due to $|F_\epsilon|^2\propto\sin^2(k_x\Delta x/2)$ term, see Eq. (41). For larger detunings, when the energy transfer $\Omega\approx\epsilon$, the relaxation rate decreases as its mostly longitudinal character that makes it $\propto(t_c/\epsilon)^2$ is combined with phonon spectral density $\propto\epsilon^3$ and piezoelectric coupling $|v^{(\mathrm{piez})}|^2\propto\epsilon^{-2}$, to produce an overall $\Gamma_-^{(\mathrm{piez})}\propto(t_c)^2/\epsilon$ scaling in the far detuned regime $\epsilon\gg t_c$, until $\epsilon\approx 500\,\mu$eV when phonon bottleneck effects start to become strongly visible. On the other hand, in Si/SiGe a weaker deformation potential scattering gives $\Gamma_\epsilon^{(\mathrm{def})}$ that first increases with ϵ and then becomes suppressed by phonon bottleneck effect at large detunings. The relaxation time $1/\Gamma_-$ falls below 100 ns for $\epsilon\sim 100\,\mu$eV only for the largest considered $t_c=40\,\mu$eV. Finally, in SiMOS the smaller interdot distance makes the transverse relaxation more efficient. Due to its $\Gamma_{t,-}^{(\mathrm{def})}\propto\epsilon^3$ scaling up to phonon bottleneck energy of about 1 meV, it becomes the dominant process at larger detunings. Such a transverse relaxation rate weakly depends on tunnel coupling (note the presence of single blue lines in Fig. 3) and requires overlap between wave functions of L/R dots, which is not large enough in the other nanostructures: $\Gamma_t^{(\mathrm{piez})}$ might be relevant in GaAs only at highest detunings, see Fig. 3(a), and the transverse process never becomes of a similar order of magnitude as the longitudinal one in the considered Si/SiGe structures.

D. Comparison of the transition rates

Let us now use the results of the previous sections and compare the relative importance of various types of environments on the discussed DQD structures. In Fig. 3, we plot the relaxation rate $\Gamma_-[\Omega(\epsilon)]$ [the excitation rate $\Gamma_+(\Omega)=\Gamma_-(\Omega)e^{-\beta\Omega}$] with solid (dashed) lines as functions of detuning for all the considered mechanisms using the above-discussed representative parameters for GaAs, Si/SiGe, and SiMOS structures, temperature $T=100$ mK and tunnel coupling $t_c=20\,\mu$eV. As expected from discussion in Sec. II C, the excitation rates are the largest at the anticrossing and they become suppressed exponentially with ϵ increasing above t_c. In that regime, the relaxation overwhelmingly dominates over excitation, but the dynamics of the electron will depend on the value of total Γ_-: the electron transfer error will depend on the ratio of timescale of environment-assisted inelastic tunneling between the dots in the far-detuned regime, $1/\Gamma_-$, and the duration of the detuning sweep. Note that for $t_c=20\,\mu$eV the requirement of $Q_{\mathrm{LZ}}<10^{-4}$ means $v<200\,\mu$eV/ns, so the total time of detuning sweep over a meV range is 5 ns. This will give a ballpark estimate what timescales we should compare $1/\Gamma_-$ to.

In GaAs, the coupling to phonons (the green line in Fig. 3 dominates the relaxation, with influence of Johnson noise possibly becoming dominant at highest considered detunings. As discussed above, $\Gamma_-^{(\mathrm{piez})}\propto t_c^2/\epsilon$ for most of the considered range of ϵ, so for the healing of the excitation to be significant the time spent at moderate detunings, up to about $200\,\mu$eV (see Fig. 3), has to be larger than average relaxation time in this range, $1/\Gamma_-\sim 1-10$ ns.

The situation is more complex in Si nanostructures. For parameters of Si/SiGe DQDs, it is the Johnson noise—red line in Fig. 3—that dominates (more visibly at lower ϵ) over the relaxation due to deformation potential coupling to phonons (the black line in Fig. 3). The detuning dependence of this process is rather weak. When $t_c/k_BT\gg 1$ (in Fig. 3, we have $t_c/k_BT\approx 2.3$), the Johnson noise from 50 Ω resistor gives $\Gamma_{-,\epsilon}^{(\mathrm{J})}\propto t_c^2/\epsilon$ for a stronger longitudinal process and $\Gamma_{-,t}^{(\mathrm{J})}\propto\epsilon$ in case of a weaker transverse one. For their assumed ratio, the relaxation rates become equal at $\epsilon_J=10\,t_c$, which means $\Gamma_-^{(J)}$ slowly decreases as ϵ^{-1} up to $\epsilon=200\,\mu$eV, and then it starts to slowly increase with $\propto\epsilon$. The relaxation time for the assumed amplitude of Johnson noise is ∼100 ns in the relevant detuning range.

Finally, for SiMOS, the smaller interdot distance assumed for this architecture makes $\Gamma_{t,-}^{(\mathrm{def})}\propto\epsilon^3$ the dominant relaxation process at large detunings: As shown in Fig. 3, this relaxation channel dominates over the one due to Johnson

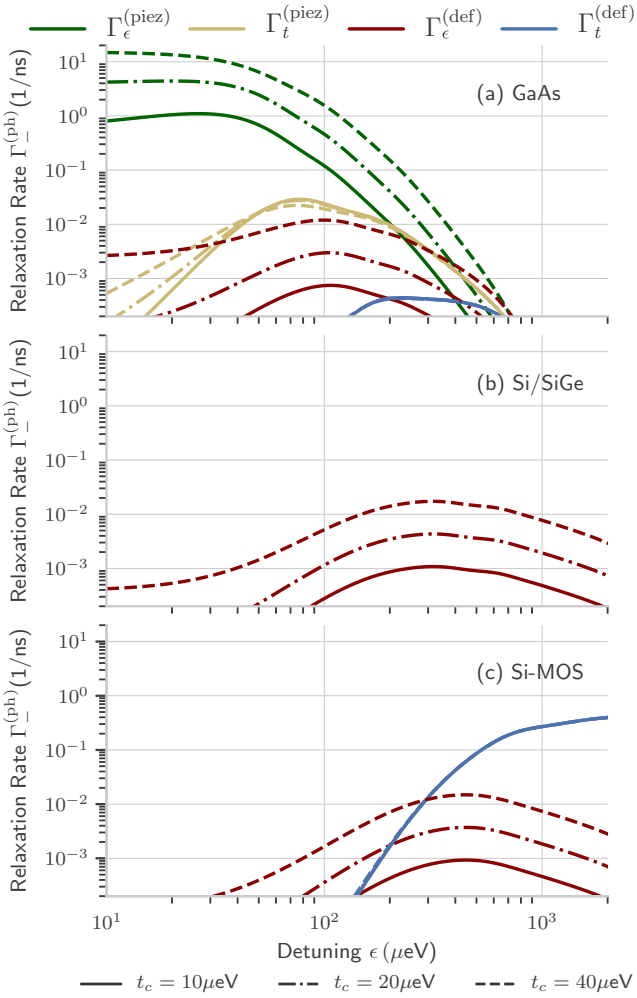

FIG. 2. Phonon relaxation rates in (a) GaAs, (b) Si/SiGe, (c) SiMOS double quantum dot devices as a function of dots detuning at fixed tunnel couplings: $t_c = 10\,\mu$eV (solid line), $20\,\mu$eV (dashed-dotted), and $40\,\mu$eV (dashed). Contributions from different phonon mechanisms are shown with a distinct color: piezoelectric longitudinal coupling $\Gamma_\epsilon^{(\mathrm{piez})}$ (green), piezoelectric transverse coupling $\Gamma_t^{(\mathrm{piez})}$ (yellow), deformation longitudinal coupling $\Gamma_\epsilon^{(\mathrm{def})}$ (red), and deformation transverse coupling $\Gamma_t^{(\mathrm{def})}$ (blue). Longitudinal phonons couples orbital-like states in vicinity of avoided crossing, while transverse phonons couples dotlike states in detuned regime. Each panel represents different device with parameters given in Table I.

noise for $\epsilon \gtrsim 200\ \mu$eV. The relaxation times at large detunings approach $\sim$10 ns, so phonon-assisted interdot tunneling might be an efficient mechanism of healing of charge noise-induced excitation that occurred close to the anticrossing in SiMOS.

The other mechanisms only weakly contribute to relaxation, as longitudinal $1/f$ noise relaxation rate is strongly attenuated with increasing detuning, as $\Gamma_{-,\epsilon}^{(1/f)} \propto t_c^2/\epsilon^3$ at $\epsilon > t_c$, while small overall strength and weak detuning dependence of longitudinal phonon processes in Si/SiGe, $\Gamma_{-,\epsilon}^{(\mathrm{def})} \propto t_c^2\epsilon$, produces relaxation times above 100 ns only approaching the order of magnitude of contribution of Johnson noise around $\epsilon = 200\,\mu$eV.

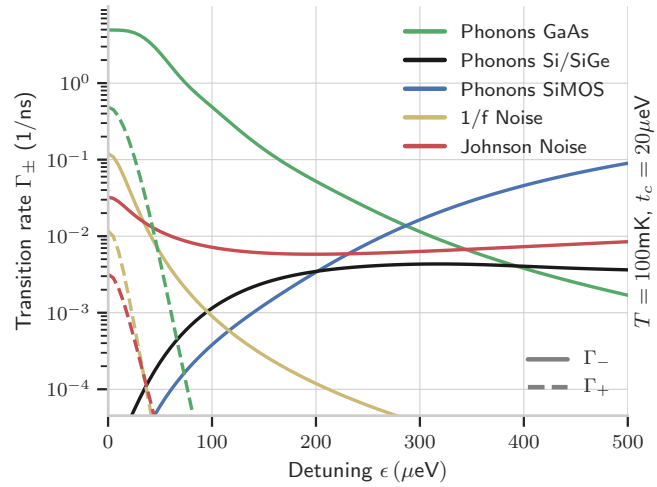

FIG. 3. Relaxation (solid lines) and excitation (dashed lines) rates as a function of detuning at typical tunnel coupling $t_c = 20\,\mu$eV and temperature of $T = 100\,$mK. Transition rates due to phonons are drawn using green (GaAs), black (Si/SiGe), and blue (SiMOS) colors, while transition rates due to common for all nanostructures charge noise is depicted using red (Johnson) and yellow ($1/f$) colors. Both excitations and relaxations in GaAs are dominated by electron-phonon coupling. In Si, the excitations are commonly caused by charge noise (either $1/f$ or Johnson of similar amplitude), while the relaxation at finite detuning relies on Johnson noise in Si/SiGe and relatively stronger interdot phonons in SiMOS, where the dots are closer.

Let us now discuss the tunnel coupling and temperature dependence of the total Γ_+ rate at $\epsilon = 0$ and of the total Γ_- rate at moderate and high detunigs, $\epsilon = 100$ and $400\ \mu$eV, respectively. The relaxation rates at moderate detuning have a common dependence on t_c inherited from the tunneling dependence of the dominant there longitudinal process, i.e., $\Gamma_- \propto t_c^2$. This is not the case at larger detuning, where transverse processes that are weakly dependent on t_c can dominate. Similarly, for the here-considered $\beta t_c \gg 1$, temperature dependence of relaxation is very weak. We illustrate both statements in Figs. 4(a) and 4(b), where we plot relaxation rates at $\epsilon = 100, 400\,\mu$eV as a function of tunnel coupling. As can be seen, the difference between Si/SiGe and SiMOS is visible at large detuning where for small tunnel couplings interdot phonons provide an order of magnitude faster relaxation rate in the latter.

In Fig. 4(c), we illustrate the relevant excitation rate $\Gamma_+(0)$, computed at the avoided-crossing at $T = 50, 100, 500\,$mK. In GaAs, the only relevant mechanism is the coupling between orbital states provided by the phonons, which has a strong scaling with tunnel coupling $\Gamma_+^{(\mathrm{piez})}(0) \propto t_c^3 e^{-\beta t_c}$ as long as $t_c \ll c/\Delta x \approx 50\,\mu$eV, where t_c^3 dependence is provided by the piezoelectric coupling (contributing a factor of t_c) and the resonance term $\sin^2(k_x \Delta x/2)$ (contributing a factor of t_c^2). As a result, at smaller temperatures, the excitation rate in GaAs shows a nonmonotonic behavior as a function of tunnel coupling. In Si, the excitation at $\epsilon \ll t_c$ is caused only by charge noise, and hence for amplitude of this noise used here for both Si/SiGe and SiMOS, it results in the same rate, in which

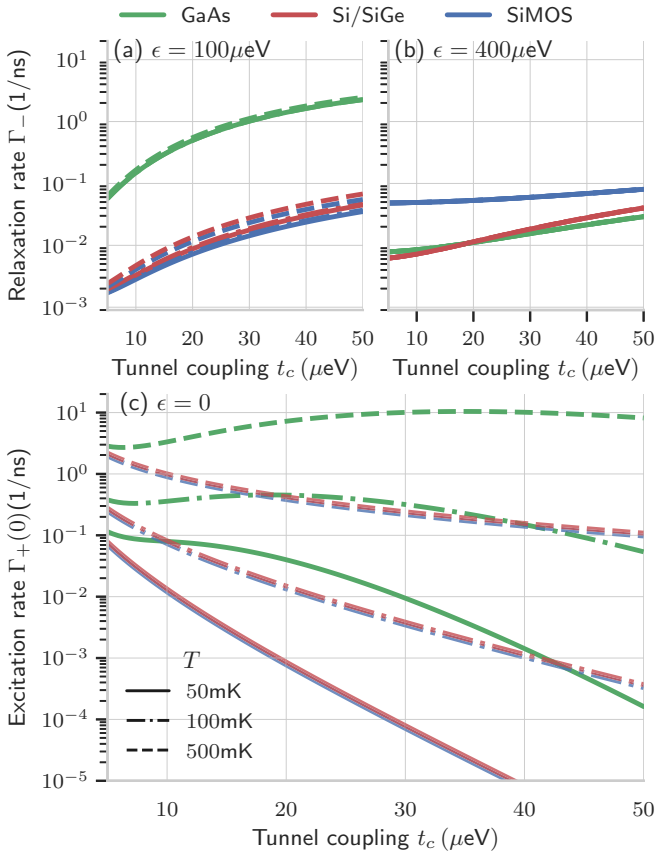

FIG. 4. Transition rates relevant for electron charge transfer in GaAs (green), Si/SiGe (red) and SiMOS (blue): the relaxation rates Γ_- at (a) $\epsilon = 100\,\mu$eV, (b) $\epsilon = 400\,\mu$eV, and (c) $\epsilon = 0$, as functions of tunnel coupling tc for temperatures $T = 50, 100, 500$ mK (solid, dashed-dotted, dashed lines, respectively). The excitation rate due to piezoelectric phonons in GaAs for $T > 100$ mK is the only nonmonotonic function of tunnel coupling. Otherwise, excitation rates decrease for larger t_c due to exponential factor $\Gamma_+(0) \propto e^{-\beta t_c}$, while relaxation rates increase due to dominant role of longitudinal mechanisms $\Gamma_-(\Omega) \propto t_c^2/\Omega^2$. Since $\Omega = \sqrt{t_c^2 + \epsilon^2}$, increase is stronger at lower ϵ. The only discrepancy between Si/SiGe and SiMOS is visible in the relaxation rate at far detuned regime ($\epsilon = 400\,\mu$eV) due to presence of interdot phonons in the latter.

contributions from $\Gamma_+^{(1/f)}(0) \propto e^{-\beta t_c}/t_c$ and $\Gamma_+^{(J)}(0) \propto t_c e^{-\beta t_c}$ are combined. The latter becomes more relevant at larger t_c, for which, however, the overall charge noise is attenuated due to exponential factor, as can be seen in Fig. 4(c) by a decrease of excitation rate in Si.

IV. PROBABILITY OF LEAVING THE ELECTRON BEHIND

Let us now use the above-derived transition rates to calculate the central quantity of this paper—occupation of higher energy state after detuning sweep Q, i.e., the probability of leaving the electron in the initial dot.

We assume the relevant part of the detuning sweep starts and terminates at $\epsilon = \pm 500\,\mu$eV, since at $\epsilon \geqslant 10t_c$ the dots become uncoupled, i.e., the approximation of constant t_c breaks down [25,105] and the detuning sweep rate used in an experiment can be increased [24]. In Fig. 5, we compare the results of a numerical solution of the AME from Eq. (10), depicted as squares, against the approximation of single excitation at avoided crossing without relaxation process, Q_{SEAL} from Eq. (15), shown as dashed lines, and the approximation of an excitation followed by relaxation processes only, Q_{HEAL} from Eq. (17), shown as solid lines. The dotted line is the LZ formula Q_{LZ} from Eq. (2). In the four panels, we show results for combinations of tunnel coupling and temperatures: $t_c = 10, 20\,\mu$eV (columns), $T = 50, 100\,m$K (rows). With hollow squares, we mark the AME results in the region where Q_{SEAL} and Q_{HEAL} are no longer an upper and lower bound on Q, as probability of LZ transition dominates. We stress that in this region the applicability of AME in secular approximation used here is limited [41,42], however, a correction to the LZ formula computed using different methods is expected to be small for predominantly longitudinal relaxation $\Gamma_\epsilon \gg \Gamma_t$ [44,50,52].

The main feature of the results of AME calculations shown by hollow and filled squares in Fig. 5 is that Q as a function of v is nonmonotonic for Si-based DQDs, while it decreases monotonically with decreasing v in GaAs-based DQDs. In Si, as we move from the highest to the lowest v, we are passing through three regions: (i) for the highest sweep rates the coherent LZ excitation determines Q, which exponentially decreases with decreasing v; (ii) at moderate v the incoherent excitations occurring close to the anticrossing due to coupling to the environment dominate Q, and $Q \propto 1/v$ as it is proportional to the time spent in the anticrossing region; and (iii) for the lowest velocities the system spends long enough time at large positive detunings for energy relaxation into the environment to suppress (heal) the excitation that occurred close to the anticrossing, and Q again starts to decrease with decreasing v. The crossover between region (i) and (ii) causes an appearance of a local minimum of $Q(v)$, while a crossover between region (ii) and (iii) leads to an appearance of wider maximum. It is clear that for parameters of GaAs-based DQD, region (ii) does not appear, and we see only a crossover between (i) and (iii) regimes. Let us now go over the quantitative $Q(v)$ behavior in more detail, starting from highest sweep rates and moving to the lowest.

In region (i), we have Q given by Q_{LZ} from Eq. (2). In region (ii), visible at lower v in both Si-based devices, we observe $Q \propto 1/v$. This suggests that the value of Q follows from a finite excitation probability in a limited range of detunings (near the anticrossing), so that the occupation of the excited state grows with increasing time spent in this region, and the subsequent relaxation in the second half of sweep time τ_∞ is negligible. In agreement with this picture, $Q \approx Q_{\text{SEAL}}$ (dashed line) and the electron undergoes a single transition from ground to excited state in vicinity of the anticrossing. Note that in Si-based devices this transition is caused solely by charge noise. The position of the local minimum of $Q(v)$ associated with crossover from regime (i) and (ii) can be estimated by finding an intersection of $Q_{\text{SEAL}}(v)$ with $Q_{\text{LZ}}(v)$, i.e.,

$$Q_{\text{SEAL}}(v_{\text{opt}}) = Q_{\text{LZ}}(v_{\text{opt}}), \tag{42}$$

the solution to which is expressed in terms of Lambert W function [106] as $v_{\text{opt}} = \pi t_c^2/2W(a)$ where $W(a)$

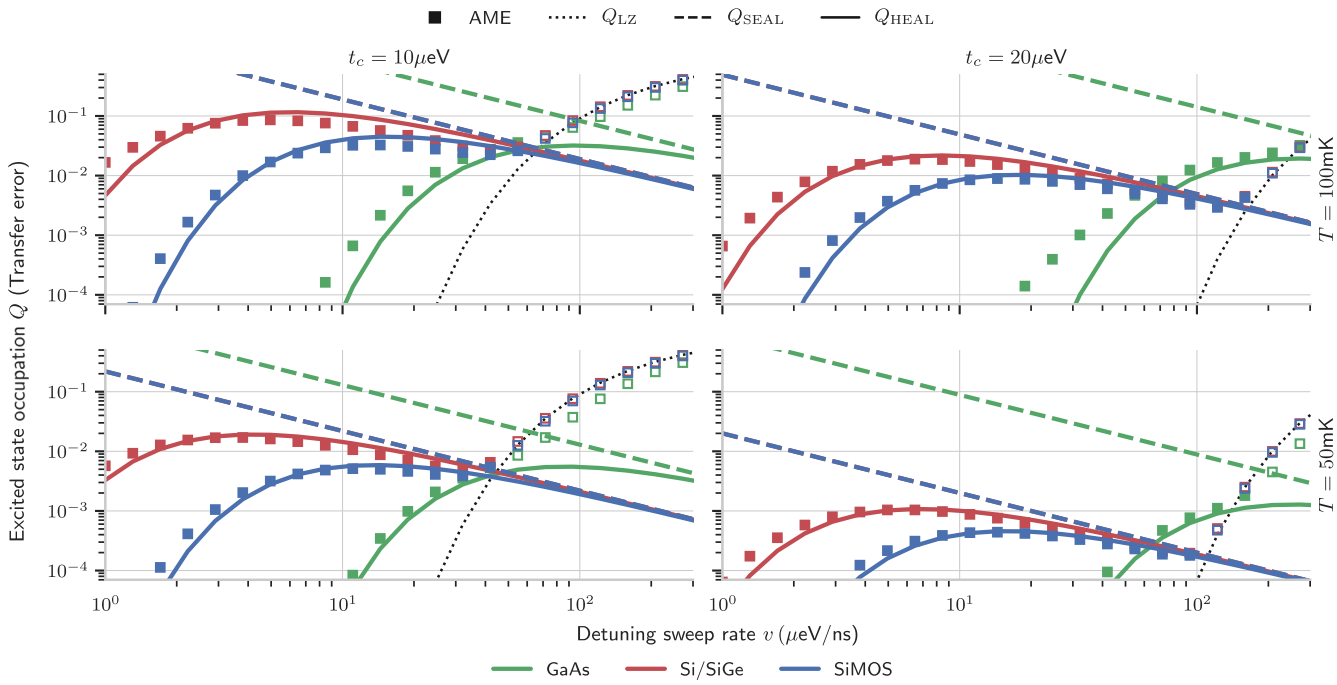

FIG. 5. Probability of occupying excited state Q, i.e., leaving the electron in the initial dot after detuning sweep, as a function of sweep rate v for fixed tunnel coupling and temperature in two semiconductor DQD devices: GaAs (green), Si/SiGe (red), and SiMOS (blue). In the four panels, we show combinations of tunnel couplings $t_c = 10, 20\mu$eV (columns) and temperatures $T = 50, 100$ mK (rows). Squares correspond to numerical solution of adiabatic master equation, where we have used filled (hollow) squares to denote adiabatic (nonadiabatic) regime. Dashed line corresponds to single excitation approximation limit Q_{SEAL}, see Eq. (16), while the solid line is the healed excitation approximation limit, Q_{HEAL}, see Eq. (17). Dotted black line shows the Landau-Zener result $Q_{\mathrm{LZ}} = \exp(-\pi t_c^2/2v)$. The remaining parameters are given in Table I.

satisfies equation $W(a)e^{W(a)} = a$ for $a = \sqrt{\frac{\pi}{8}}\sqrt{\beta t_c^3}/\Gamma_+(0)$. Since typically $a \gg 1$, the asymptotic form of $W(a) \sim \ln(a) - \ln(\ln(a))$ allows us to quantitatively reproduce $v_{\mathrm{opt}} \approx 45(75)\,\mu$eV/ns at $t_c = 10\,\mu$eV and $v_{\mathrm{opt}} \approx 115\ (170)\ \mu$eV/ns at $t_c = 20\,\mu$eV for $T = 50\ (100)$ mK, respectively, using parameters from Fig. 5. At very low temperature, at which $\ln(a) \propto t_c$ the linear scaling $v_{\mathrm{opt}} \propto t_c$ is expected, as can be seen in Fig. 7(a) for $T = 50$ mK and $t_c \leqslant 50\,\mu$eV.

As the sweep rate is decreased, we enter the region (iii): An increasing time spent during the electron transfer in the far-detuned regime, $\epsilon \gg t_c$, allows for a significant recovery of ground-state occupation by the relaxation mechanism, which is reflected by a deviation from a SEAL approximation and $Q \approx Q_{\mathrm{HEAL}}$ (solid lines) for the smallest sweep rates. The healing effect is stronger for the SiMOS device, due to effective phonon relaxation between the dotlike eigenstates at large detunings. The agreement between the result of the evaluation of AME and the approximation is more visible at lower T (higher t_c), since this agreement is expected to improve as $t_c/k_{\mathrm{B}}T \gg 1$. According to Eq. (17), the healing effect becomes significant when $\int_0^{\tau_\infty} \Gamma_-(\tau)d\tau \approx 1$. Using this condition, we estimate the value of v_{max} at which a crossover between regimes (ii) and (iii) occurs, and $Q(v)$ exhibits a local maximum. For a relaxation rate of $\widetilde{\Gamma}_- = 10^{-2}\,\mathrm{ns}^{-1}$ typical for Si/SiGe devices (see Fig. 3) we obtain $v_{\mathrm{max}} \approx 5\mu$eV/ns, which agrees nicely with results shown in Fig. 5. For SiMOS, v_{max} is visibly shifted to higher v due to, caused by smaller distance between the dots, stronger coupling to deformation phonons, i.e., $\Gamma_-(\epsilon > 200\,\mu\mathrm{eV}) > 10^{-2}\,\mathrm{ns}^{-1}$. Crucially, the values of v_{max} for Si-based devices are below v_{opt} given above,

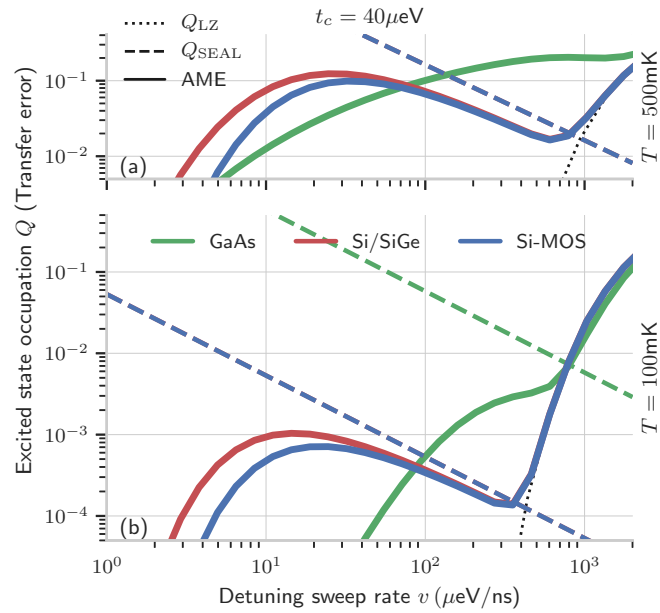

FIG. 6. Probability of leaving the electron behind in the case of high tunnel coupling $t_c = 40\mu$eV. We compare results for $T = 500$ mK (a) and $T = 100$ mK (b), since large tunnel coupling in general should allow for relatively efficient transfer in higher temperature.

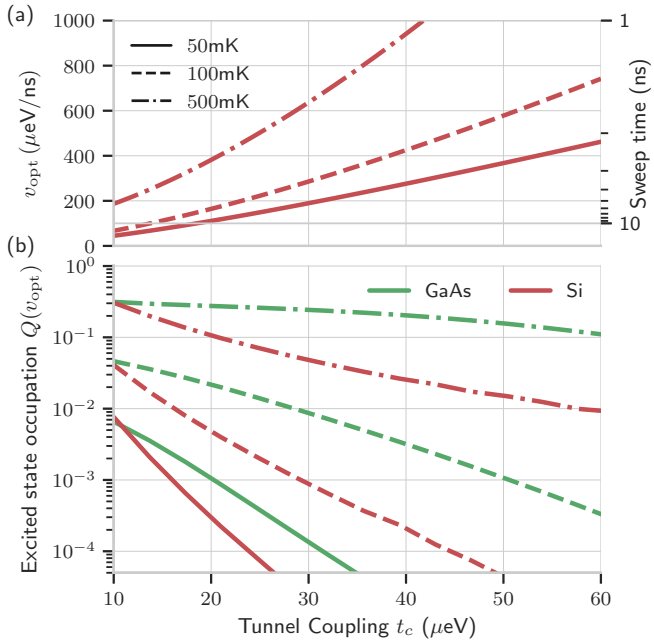

FIG. 7. Optimal transfer in Si. In panel (a), we plot optimal sweep rate for Si/SiGe and SiMOS devices $v_{\rm opt}$ obtained as a solution to Eq. (42) for $T = 50, 100, 500$ mK (solid, dashed and dotted-dashed lines). In panel (b), we plot probability of leaving the electron behind after the detuning sweep with a rate $v_{\rm opt}$, as a function of tunnel coupling t_c and for the same selection of temperatures. We compare results for Si against phonon dominated transfer with the same sweep rate in GaAs (green) as a reference.

and consequently region (ii) actually exists for these devices. This is not the case for GaAs DQDs considered here: A much faster relaxation $\widetilde{\Gamma}_- \sim 1\,\mathrm{ns}^{-1}$ due to piezoelectric coupling to phonons results in $v_{\rm max} \sim 500\,\mu$eV/ns, that is, $\gg v_{\rm opt}$, so in GaAs region (i) crosses over directly to (iii), and $Q(v)$ is a monotonic function. The agreement between the AME calculation and the $Q_{\rm HEAL}(v)$ approximation is good as long as $Q_{\rm SEAL}(v) \leqslant 0.1$, i.e., the probability of excitation-relaxation-excitation sequence is relatively low ($<Q^2_{\rm SEAL}$). However, when the electron transfer time is long enough to allow for a second transition from ground to excited state, i.e., when $Q_{\rm SEAL} \geqslant 0.1$, the HEAL formula gives only a lower bound for results of the AME, as visible at low v when comparing the squares and solid lines.

The transition from nonmonotonic behavior of $Q(v)$ in Si to a monotonic one in GaAs is clearly caused by increased coupling to the environment. This agrees with Ref. [53], where a transition from nonmonotonic to monotonic behavior of Q as a function of coupling strength was shown. In general, since the relaxation rate is proportional to the coupling squared, i.e., $\Gamma \propto \mathcal{V}^2$ (see Eqs. 19 and 20) the nonmonotonic behavior in GaAs would require approximately two times weaker coupling to phonons, while monotonic behavior in Si would need about four times stronger coupling to charge noise or phonons.

An obvious way to increase the efficiency of charge transfer (increase Q) is to bring the $Q_{\rm SEAL}$ result down, as for $\Gamma_+ < \Gamma_-$ it gives an upper bound of excited-state occupation induced by environmental fluctuations, i.e., $Q < Q_{\rm SEAL}$ in the adiabatic regime where $Q > Q_{\rm LZ}$. This can be achieved by lowering the temperature or increasing the tunnel coupling. In Fig. 6, we show a rather optimistic result of probability of leaving the electron in the left dot evaluated for the largest t_c reported in the array of Si/SiGe QDs [24], $t_c = 40\,\mu$eV. As a reference, we compare it to the other materials considered, and plot results for $T = 100, 500$ mK, as larger tunnel couplings should in principle allow for working at higher temperatures [107–109]. We stress that a calculation for $T = 50$ mK (not shown) gives $Q \leqslant 10^{-6}$ for $v < 400\,\mu$eV/ns. For Si nanostructures, the behavior at higher temperatures is qualitatively similar to than shown in Fig. 5, with a local minimum of $Q = 10^{-4}, 10^{-2}$ at $v = 400\,\mu$eV/ns, $800\,\mu$eV/ns for $T = 100,\ 500$ mK, respectively. In GaAs, the large value of t_c results in strong coupling between transferred electron and the environment, which at higher temperatures causes flattening of Q as a function of v. This effect can be attributed to reaching thermal equilibrium of $Q_{\rm eq}(\epsilon = 0) = \Gamma_+(0)/(\Gamma_+(0) + \Gamma_-(0)) \sim 0.3$ around the avoided crossing, followed by slower relaxation at larger ϵ.

While using very small v guarantees very small Q, making the electron charge transfer too slow will eventually have a negative effect on coherence of its spin, see the next section for discussion. In Si-based devices, using $v \approx v_{\rm opt}$, which gives Q smaller than those that can be obtained with v up to two orders of magnitude smaller, is thus a good choice when fast and coherent spin qubit shuttling is required. In Fig. 7(a), we show how $v_{\rm opt}$ in Si varies with t_c for $T = 50, 100, 500$ mK. We see that $v_{\rm opt}$ increases as the $Q_{\rm LZ}$ curve shifts to higher v (due to an increase of t_c), or noise-induced excitations $Q_{\rm SEAL}$ become stronger (here due to an increase of T). Next, in Fig. 7(b), we use $v_{\rm opt}$ to compare the corresponding transfer error in Si $Q(v_{\rm opt})$ (red) against analogous quantity in GaAs (green), as a function of $t_c \in 10 - 60\,\mu$eV. In the figure, we have put together results of the AME (solid, dashed, dotted dashed lines) for three different temperatures $T = 50, 100, 500$ mK. The probability of losing the electron Q in SiGe appears to be below the value of GaAs for considered tunnel couplings. For smaller $t_c \leqslant 10\,\mu$eV, we would expect $v_{\rm opt} \leqslant 50\,\mu$eV, however, treatment of this regime lays behind the scope of this paper (AME method), as in this case, and in particular in GaAs, the LZ-dominated part $v > v_{\rm opt}$ is significantly modified by the relaxation. Of course, Q in GaAs can be made lower by using $v < v_{\rm opt}$, but there are other factors that are limiting v from below in GaAs devices (see discussion in the next section). Similarly, in Si QDs charge transfer can, in principle, be improved by going to much lower sweep rates $v < 1\mu$eV/ns, however, it would make the few-nanosecond transfer impossible as it has been demonstrated by showing the sweep time interval on the right y axis of Fig. 7(a).

The value of optimal sweep rate and corresponding minimum of transfer error $Q(v_{\rm opt})$ in Si depends on the amplitude of charge noise at frequency corresponding to tunnel coupling (which is in the GHz range), where its influence dominates over that of phonons. We concentrate here on the amplitude of $1/f$ noise, the amplitude of which can vary by at least an order of magnitude between different Si DQD devices. In Fig. 8, we plot a minimal transfer error at typical electron temperature $T = 100$ mK as a function of square root of

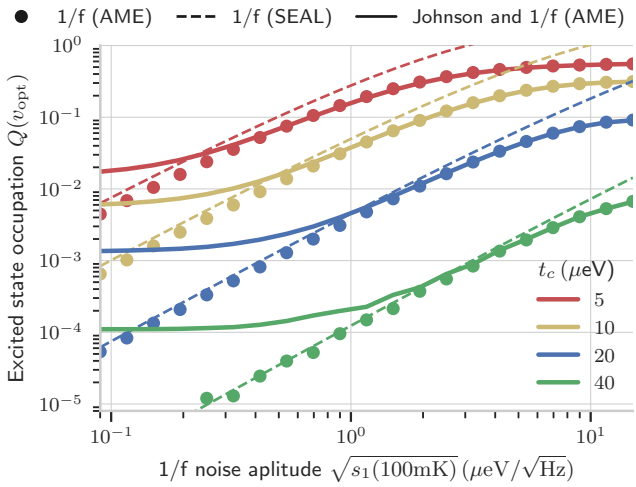

FIG. 8. Probability of leaving the electron behind using optimal sweep rate v_{opt}, as a function of $1/f$ noise spectral density measured at 1 Hz and selection of tunnel couplings $t_c = 5, 10, 20, 40\,\mu$eV at $T = 100\,$mK. For that assumed in the Sec. III B model of high-frequency $1/f$ noise, we compare results of adiabatic master equation with (solid line) and without (dots) additional contributions from Johnson noise against Q_{SEAL} approximation with $1/f$ noise only (dashed lines). For the noise in tunnel couplings, we assumed $s_1^t = (0.1)^2 s_1^\epsilon$.

$1/f$ spectral density evaluated at 1 Hz and at $T = 100\,$mK, which we have previously taken as constant $\sqrt{s_1(100\,\text{mK})} = 1\,\mu\text{eV}/\sqrt{\text{Hz}}$ (see Sec. III B). We plot the results for the range of t_c considered here and emphasize that noise amplitude can be directly related to excitation rate at $\Omega = t_c$ with the following formula:

$$\Gamma_+^{(1/f)}(t_c)[1/\text{ns}] \approx \frac{2s_1[\mu\text{eV}^2/\text{Hz}]}{t_c[\mu\text{eV}]} \exp\left(-\frac{t_c}{k_B T}\right), \qquad (43)$$

where $s_1 = s_1(100\,\text{mK})$ for brevity and square brackets denoted units in which the quantities should be substituted. The excitation rate obtained using this equation can be directly used in the SEAL formula, given by Eq. (16), the result of which was illustrated in Fig. 8 using dashed lines. As expected, Q_{SEAL} agrees well with the results of AME (dots) for relatively small error $Q(v_{\text{opt}}) \ll 1$. Next we analyze the transition between $1/f$ and Johnson noise dominated excitations. The latter can be seen in Fig. 8 as a flattening of the solid lines, which represents results of the AME with both $1/f$ and Johnson noise, from $R = 50\,\Omega$ resistor, contributions. By comparing solid and dashed lines, we conclude that amplitude of $1/f$ noise at which it starts to dominate over Johnson noise becomes larger when the tunnel coupling is increased, which can be deduced from the scaling of respective excitation rates, i.e., $\Gamma_+^{(1/f)}(t_c) \propto 1/t_c$ and $\Gamma_+^{(J)}(t_c) \propto t_c$ for $t_c \gg k_B T$. As the optimal sweep rate v_{opt} is too high to allow for any phonon-mediated suppression of Q in Si DQDs, the difference between AME and SEAL visible for large noise amplitude is attributed to subsequent relaxation (and further transitions) caused by $1/f$ noise of either large amplitude ($t_c \geqslant 10\,\mu$eV) or at relatively high temperature ($t_c = 5\,\mu$eV, for which $\beta t_c \sim 0.5$).

V. DISCUSSION AND SUMMARY

We have presented a theory of the dynamics of a system undergoing a LZ transition in the presence of weak transverse and longitudinal couplings to thermal environments: sources of noise of $1/f$ and Johnson types, and a bath of noninteracting bosons, specifically, acoustic vibrations of a three-dimensional crystal. Our focus was on the regime in which the deterministic change of parameters of the Hamiltonian is slow enough to neglect the LZ coherent excitation, and the effectively nonadiabatic character of the evolution can be caused only by interaction with the environment. A general theory based on AME was then applied to a case of electron transfer between a pair of voltage-controlled semiconductor QDs, for which we took into account realistic parameters for electron-phonon interaction and both Johnson and $1/f$ charge noise. We have calculated transition rates between a system's eigenstates as a function of interdot detuning ϵ, and used them in AME calculation to obtain the probability of the failure of charge transfer between the two dots, Q, as a function of detuning sweep rate v.

When v is below the value at which the LZ transition is activated, only a finite temperature of environment allows for energy absorption necessary for modification of Q, since otherwise electrons would stay in the ground state. This absorption most likely takes place in the vicinity of the anticrossing, where the thermal energy needed for transition is the smallest. A specific feature of the system under consideration is that the dominant coupling to the environment is most effective at the anticrossing, making this effect even stronger. Consequently, during the process of electron transfer caused by sweeping the detuning, a finite Q is generated at the anticrossing, when $|\epsilon| \leqslant t_c$. Then, for larger positive detunings the electron relaxation processes dominate over the excitation processes and suppression of Q is expected.

In the considered DQDs, there are two possible scenarios. In Si-based dots, coupling to charge noise dominates, and the transition timescales are longer than the typical transfer times, so the final Q is very close to the value generated near the anticrossing, which is $\propto 1/v$ (proportional to the time spent near the anticrossing), so it exhibits a dependence on v qualitatively opposite to the one for LZ effect dominating at large v. Only at lowest v the energy relaxation starts to be efficient at lowering Q, with this effect being stronger in SiMOS compared to Si/SiGe structures. The competition between the environment-induced excitation and LZ effect leads then to appearance of optimal v, at which Q is minimal. In GaAs, on the other hand, a strong piezoelectric coupling to phonons dominates, transition timescales are shorter than the charge transfer time, and, consequently, many transitions take place and the final Q monotonically decreases with decreasing v, approaching a value exponentially small in final ϵ, reflecting approaching a thermal occupation of the ground state.

The main qualitative theoretical result of the paper, which could also apply to systems other than double QDs, is thus that a system described by a LZ model, when coupled to a thermal environment can realize two possible scenarios: one qualitatively similar to the LZ effect but with dependence of Q on v renormalized by environment, and another in which dependence of Q on v is nonmonotonic, and there is an

optimal sweep rate that minimizes Q. The main conclusion specific to the considered case of GaAs and Si-based QDs is that for $T \approx 50$ mK, in the GaAs case Q can be made smaller than 10^{-4} by choosing v smaller than ≈ 10 (100) μeV/ns for $t_c = 10$ (20) μeV, while in the case of Si having $Q = 10^{-4}$ requires $t_c > 20$ μeV, and optimal v of a few tens of μeV/ns. Large tunnel couplings and low temperatures are crucial for having small Q. In Si-based DQDs, there is a possibility of further suppression of Q by decreasing the level of charge noise at GHz frequencies, corresponding to $t_c \approx 10$ μeV energy splitting at the anticrossing.

A process of a controlled electron transfer between two QDs is relevant for ongoing attempts at construction of quantum buses based on chains of many tunnel-coupled dots [22,24,27,39,70]. Let us now discuss the implications of the results of this paper for prospects of coherent shuttling of electron-based spin qubits across $N \approx 100$ QDs. This number of dots in a 1D chain is motivated by the requirement of having ≈ 10 μm distance between few-qubit registers in a realistic architecture of a quantum computer based on gate-controlled QDs [9] and typical interdot separation $\lesssim 100$ nm.

When the goal of charge shuttling is an on-demand transfer of qubits, which should be highly coherent and which are to take part in further coherent manipulations after being moved from one register to another, the deterministic character of the shuttling is necessary. Any randomness in qubit arrival times will complicate the application of subsequent coherent operations involving that qubit. Furthermore, any stochastic component in the duration of the qubit transfer will introduce a random contribution to the phase of the qubit. More in-depth discussion of the relationship between the indeterministic character of electron shuttling and spin qubit dephasing is given in Ref. [70]; here it is enough to realize that large probability of electron arriving at the end of N-dot chain at a time other than the desired one will cause major problems in the context of quantum information processing and we will treat it here as an error probability. Assuming that $Q \ll 1/N$, the probability of the electron arriving at the end of the chain *not* at the desired time, i.e., the probability of qubit transfer-associated error is $Q_N \approx NQ$.

Our results for Si-based QDs show that for tunnel couplings in the $5-40$ μeV range, as recently reported in first experimental realizations of electron shuttling over a few dots, achieving $Q_N \approx 10^{-3}$ will be possible for $t_c \geqslant 30$ μeV and at $T \leqslant 50$ mK. It should be stressed that a finite variance of distribution of t_c is expected due to unavoidable electrostatic disorder in gated and doped heterostructure, so even with average tunnel coupling larger than a given value, there is a finite probability of having at least a pair of neighboring dots characterized by a much smaller t_c. As one can see in Fig. 7(b), transfer errors associated with such a weakly tunnel-coupled pair can completely dominate the error for the whole chain of QDs. Note that a high-fidelity charge transfer between two dots in Si MOS structures was demonstrated experimentally using $t_c = 450$ μeV [27], but maintaining such a strong tunnel coupling in a 1D array of $N \approx 100$ QDs will be challenging.

In GaAs, on the other hand, Q_N can be made much smaller by decreasing the detuning sweep rate v, so the time of interdot transfer becomes longer than ~ 10 ns. This, in fact, also holds for Si-based dots, only v has to be made at least a further order of magnitude smaller. However, for such slow transfers one has to start worrying about well-known mechanisms of spin dephasing that affect the coherence of a static electron localized in a QD. In both considered materials, interaction with nuclei leads to dephasing T_2^* time of the order or 10 ns for GaAs [110] and a few hundreds of ns for natural Si [111–113] (and up to tens of microsecond for isotopically purified silicon with about 10^3 ppm of spinful ^{29}Si [81,111,114]). For isotopically purified Si QDs in vicinity of micromagnets, their spatially inhomogeneous magnetic fields together with charge noise lead to $T_2^* \approx 20$ μs. Let us now use $T_2^* = 10$ ns (10 μs) for GaAs and Si. To avoid significant spin dephasing during the interdot charge transfer, the time of the latter has to be much shorter than T_2^*. Assuming that the range of detuning sweep corresponding to the transfer is ~ 1 meV, the sweep rates have to fulfill $v \gg 0.1$ μeV/ns for Si, and $v \gg 100$ μeV/ns in GaAs. In Fig. 5, we see that it means that in GaAs this lower bound on v severely restricts the possibility of lowering Q by making the transfer slower, and in fact a tradeoff between amount of spin dephasing and a finite value of Q due to LZ effect that dominates the behavior of $Q(v)$ for $v \geqslant 100$ μeV/ns has to be made. In silicon, the lower bound on v is much smaller than v_{opt}, so a local minimum of Q visible in the figure is attainable—but the viability of strategy of lowering Q by using $v < 1$ μeV/ns depends on the efficiency of electron relaxation due to charge noise and electron-phonon relaxation (compare red and blue lines, corresponding to Si/SiGe and SiMOS in the figure) and an exact value of T_2^*. All these observations suggest that from the point of view of coherent transfer of a spin qubit, Si-based QD architectures could have an advantage over GaAs-based ones.

Let us finish by stressing the main message following from our calculations for realistic GaAs and Si-based QDs: The dynamics of interdot electron transfer is very strongly affected by electron's interaction with charge noise in Si-based systems and phonons in case of GaAs-based ones. Effects of energy exchange with these environments have to be taken into account to correctly describe the basic physics of electron transfer in currently available devices. More subtle effects appearing in closed-system descriptions, associated with spin-orbit and valley-orbit (in case of Si) interactions [29,30,34,35,39,70], will make the physics of charge transfer, and especially of coherent spin transfer, even richer, but interaction with charge noise and phonons is a crucial element of description of dot-to-dot electron transfer for low and moderate detuning sweep rates.

ACKNOWLEDGMENTS

We would like to thank Lars Schreiber and Lieven Vandersypen for discussions that motivated us to focus on the problem addressed in the paper, and Piotr Szańkowski for multiple comments on earlier versions of this paper. This work has been funded by the National Science Centre (NCN), Poland under QuantERA program, Grant No. 2017/25/Z/ST3/03044. Project Si-QuBus has received funding from the QuantERA ERA-NET Cofund in Quantum Technologies implemented within the European Union's Horizon 2020 program. J.A.K. acknowledges fi-

nancial support from the National Science Centre (NCN), Poland under the ETIUDA doctoral scholarship (Grant No. 2020/36/T/ST3/00569).

APPENDIX A: CORRECTION DUE TO DYNAMICS OF CLASSICAL NOISE

Here we provide detailed calculations of occupation of the excited state in the classical limit, i.e., where the fluctuations of detuning and tunnel coupling can be modeled by stochastic contribution to Hamiltonian Eq. (1), i.e.,

$$\hat{H} = \frac{\epsilon + \delta\epsilon}{2}\hat{\sigma}_z + \frac{t + \delta t}{2}\hat{\sigma}_x. \tag{A1}$$

As pointed out in the main text, in the limit of weak noise corrections come from noise dynamics, which in the adiabatic frame modifies off-diagonal element of Hamiltonian Eq. (6), written explicitly as

$$\dot{\theta} \approx \frac{\sin\theta\delta\dot{\epsilon} + \cos\theta\delta\dot{t}}{\Omega_0}, \tag{A2}$$

where $\Omega_0 = \sqrt{\epsilon^2 + t_c^2}$, $\cos\theta = -\epsilon/\Omega_0$, $\sin\theta = t_c/\Omega_0$, and $\delta\dot{\epsilon} = \partial_\tau\delta\epsilon$.

1. Leading order perturbation theory

We evaluate the leading order excitation probability $Q^{(1)}$ due to the noisy term. We use first-order time-dependent perturbation theory in the adiabatic basis $|\tilde{\psi}(\tau)\rangle = a_-(\tau)|-,\theta\rangle + a_+(\tau)|+,\theta\rangle$ and, assuming $a_+ = \lambda a_+^{(1)} + \lambda^2 a_+^{(2)} + \ldots$, we compute in leading order the correction to occupation of excited state as $Q^{(1)} = \langle|a_+^{(1)}(\tau)|^2\rangle$, which equals

$$Q^{(1)} = \frac{1}{4}\int_{-\infty}^{\infty}\langle\dot{\theta}(\tau_1)\dot{\theta}(\tau_2)\rangle\, e^{i\int_{\tau_2}^{\tau_1}\Omega_0(\tau')d\tau'}d\tau_1 d\tau_2, \tag{A3}$$

where $\langle\ldots\rangle$ denotes classical averaging over noise realizations. The substitution of Eq. (25) into Eq. (A3) results in four distinct contributions:

$$Q^{(1)} = Q_{\epsilon\epsilon}^{(1)} + Q_{tt}^{(1)} + Q_{\epsilon t}^{(1)} + Q_{t\epsilon}^{(1)}, \tag{A4}$$

which correspond to auto- or cross-correlation function of respective noise derivative $Q_{xy}^{(1)} \sim \langle\delta\dot{x}(\tau_1)\delta\dot{y}(\tau_2)\rangle$, where $x, y = \epsilon$ or t. For assumed here stationary noises, it is convenient to use the Fourier transform of correlation function, which for the noise derivative can be expressed in terms of power spectral density of noise $S_{xy}(\omega) = \int_{-\infty}^{\infty}\langle\delta x(\tau)\delta y(0)\rangle e^{-i\omega\tau}d\tau$, i.e. $S_{\dot{x}\dot{y}}(\omega) \equiv \omega^2 S_{xy}(\omega)$ [75]. This allows us to write the correction as

$$Q_{xy}^{(1)} = \int_{-\infty}^{\infty}\frac{d\omega}{8\pi}S_{xy}(\omega)\,F_x(\omega)F_y^*(\omega), \tag{A5}$$

in which we introduced filtering function $F_x(\omega)$ using Eq. (A3),

$$F_x(\omega) = \int_{-\infty}^{\infty}d\tau\, f_x(\tau)\frac{\omega}{\Omega(\tau)}\exp\left(i\omega\tau + i\int_0^\tau\Omega(\tau')d\tau'\right), \tag{A6}$$

with $f_\epsilon(\tau) = \sin\theta = t_c/\Omega$ and $f_t(\tau) = \cos\theta = -v\tau/\Omega$.

2. Stationary phase approximation

We evaluate the integral Eq. (A6) for $x = \epsilon, t$, in leading order of stationary phase approximation, where we seek for time at which the argument of exponent $\varphi(\tau) = \omega\tau + \int_0^\tau\Omega(\tau')d\tau$ is stationary, i.e., $\partial_\tau\varphi(\tau) = 0$, from that $\omega = -\Omega(\tilde{\tau})$, which takes place at $\pm\tilde{\tau} = \sqrt{(\omega^2 - t_c^2)/v^2}$. Additionally, since $\Omega \geqslant t_c$, the ω is strictly negative and smaller then $-t_c$. The second derivative of the phase evaluated at $\tilde{\tau}$ reads $\partial_\tau^2\varphi(\tau)|_{\tau=\tilde{\tau}} = \pm v\sqrt{1 - t_c^2/\omega^2}$. In leading order, the integral Eq. (A6) reads

$$F_\epsilon \approx \frac{t_c}{\omega}\int_{-\infty}^{\infty}\exp\left[i\varphi(\tilde{\tau}) + i\frac{v}{2}\sqrt{1 - t_c^2/\omega^2}(\tau - \tilde{\tau})^2\right] + \exp\left[i\varphi(-\tilde{\tau}) - i\frac{v}{2}\sqrt{1 - t_c^2/\omega^2}(\tau + \tilde{\tau})^2\right]d\tau, \tag{A7}$$

$$F_t \approx \frac{-v\tilde{\tau}}{\omega}\int_{-\infty}^{\infty}\exp\left[i\varphi(\tilde{\tau}) + i\frac{v}{2}\sqrt{1 - t_c^2/\omega^2}(\tau - \tilde{\tau})^2\right] - \exp\left[i\varphi(-\tilde{\tau}) - i\frac{v}{2}\sqrt{1 - t_c^2/\omega^2}(\tau + \tilde{\tau})^2\right]d\tau. \tag{A8}$$

Now we perform Gaussian integration, $\int dx e^{iax^2} = \sqrt{\frac{\pi}{ia}}$, using which integrand terms differ by a phase $\sqrt{1/\pm i} = e^{\mp\pi/4}$. Since $\varphi(\tilde{\tau}) = -\varphi(-\tilde{\tau})$, the result can be written as

$$F_\epsilon(\omega) = \frac{2t_0\cos(\varphi(\tilde{\tau}) - \pi/4)}{\omega}\sqrt{\frac{2\pi}{v}}\left(1 - \frac{t_c^2}{\omega^2}\right)^{-1/4},$$
$$F_t(\omega) = \frac{-2iv\tilde{\tau}\sin(\varphi(\tilde{\tau}) - \pi/4)}{\omega}\sqrt{\frac{2\pi}{v}}\left(1 - \frac{t_c^2}{\omega^2}\right)^{-1/4}. \tag{A9}$$

First, we consider diagonal part ($x = y$) of Eq. (A5), in which $|F_\epsilon|^2 \propto \cos^2(\varphi - \pi/4)$ and $|F_t|^2 \propto \sin^2(\varphi - \pi/4)$. Due to the rapidly oscillating nature of both functions, we replace them by average values of $\cos^2\varphi$ and $\sin^2\varphi$ equal $1/2$, which leads to

$$Q_{\epsilon\epsilon}^{(1)} = \frac{1}{2v}\int_{-\infty}^{-t_c}d\omega S(\omega)\frac{t_c^2}{\omega^2}\left(1 - \frac{t_c^2}{\omega^2}\right)^{-1/2},$$
$$Q_{tt}^{(1)} = \frac{1}{2v}\int_{-\infty}^{-t_c}d\omega S(\omega)\frac{\omega^2 - t_c^2}{\omega^2}\left(1 - \frac{t_c^2}{\omega^2}\right)^{-1/2}, \tag{A10}$$

where the strictly negative value of ω reflects absorption of energy quanta. Finally, we conclude by showing that cross correlation is negligibly small. We use the argument that $F_t^* = -F_t$ is strictly imaginary and, as a result, we have

$$Q_{\epsilon t}^{(1)} + Q_{t\epsilon}^{(1)} = \int_{-\infty}^{\infty}(S_{\epsilon t}(\omega) - S_{t\epsilon}(\omega))F_\epsilon(\omega)F_t^*(\omega), \tag{A11}$$

where the integrand is equivalent to the imaginary part of the cross spectrum, and hence vanishes for $\langle\delta\epsilon(\tau)\delta t(0)\rangle = \langle\delta t(\tau)\delta\epsilon(0)\rangle$. The nontrivial imaginary part of the cross-spectrum results only from causal relation between δt, $\delta\epsilon$ [94], however, even in such a special case we argue that $F_\epsilon(\omega)F_t^*(\omega) \propto \cos(\varphi + \pi/4)\sin(\varphi + \pi/4)$ which, due to zero average, is expected to be much smaller than auto-correlation contributions. As a result, corrections to occupation of the excited state due to weak classical noise can

be written as

$$Q^{(1)}_{\epsilon\epsilon} = \frac{1}{2v}\int_{t_c}^{\infty} d\Omega \frac{S_\epsilon(-\Omega)}{\sqrt{1-t^2/\Omega^2}}\left(\frac{t_c^2}{\Omega^2}\right),$$
$$Q^{(1)}_{tt} = \frac{1}{2v}\int_{t_c}^{\infty} d\Omega\, S_t(-\Omega)\sqrt{1-\frac{t_c^2}{\Omega^2}}, \qquad \text{(A12)}$$

using which we recovered high frequency limit of Ref. [61], where the lower bound of the integrals reflects the minimal energy needed for the excitation to occur. Due to the dominant role of longitudinal component $\delta\epsilon$, we omit here contributions from frequencies below t_c, which are relevant only for transverse δt noise [60,61]. In particular, corrections from quasistatic noise in tunnel coupling vanishes in assumed here weak noise ($\delta t \ll t_c$) and adiabatic ($t_c^2 > v$) limits [57].

3. Transition rates

The first-order calculation can be interpreted as a probability of a single transition fromthe ground to excited state during adiabatic transfer, and as such can be written as an integral of transition rate $Q^{(1)} = \int d\tau' \Gamma_\infty(\tau')$, see Eq. (15). An explicit form of Γ_∞ can be deduced from Eq. (A12) as

$$\Gamma_{\infty,\epsilon}(\tau) = \frac{1}{4}\left(\frac{t_c}{\Omega(\tau)}\right)^2 S^{\rm cl}_\epsilon(\Omega(\tau)),$$
$$\Gamma_{\infty,t}(\tau) = \frac{1}{4}\left(1-\left(\frac{t_c}{\Omega(\tau)}\right)^2\right) S^{\rm cl}_t(\Omega(\tau)). \qquad \text{(A13)}$$

Finally, we prove that a result obtained by substituting $\Gamma_\pm = \Gamma_\infty = \Gamma_{\infty,\epsilon} + \Gamma_{\infty,t}$ into rate equation Eq. (12), which results in high temperature solution,

$$Q^{(\infty)} = \frac{1}{2}\left(1-\exp\left(-2\int_{\tau_i}^{\tau_f}\Gamma_\infty(\tau')d\tau'\right)\right), \qquad \text{(A14)}$$

equivalent to an evolution driven by Hamiltonian Eq. (1), averaged over realizations of classical fluctuations of parameters. In Fig. 9, we have separately plotted contributions from detuning noise $\delta\epsilon$ (solid line) and tunnel coupling noise δt (dashed line), as a result of $1/f$ noise (hollow dots) and white noise (filled dots). Independently of the considered noise type, in the fast sweep rate limit ($v \gg t_c^2$) we recover the LZ solution, for which $Q_{\rm LZ}$ depends on the relation between v and t_c only, and thus for sufficiently large v the results group according to tunnel couplings $t_c = 10\,\mu$eV (green) and $t_c = 20\,\mu$eV (red). In the low sweep rate limit, for $1/f$ noise in detuning (solid line, hollow dots), we obtain results from Ref. [38], for which $Q^{(\infty)}_\epsilon$ ($Q^{(\infty)}$ with $\Gamma_\infty = \Gamma_{\infty,\epsilon}$) is independent of t_c. The same applies to $1/f$ noise in tunnel coupling (dashed lines, hollow dots), for which a tenfold decreased noise amplitude (compared to the case of detuning noise) translates into almost two orders of magnitude lower $Q^{(\infty)}_t$. For the white part of Johnson's noise, distinction between different t_c is much more visible for noise in detuning (solid lines, filled dots), since larger t_c significantly increases the time spent in the vicinity of avoided crossing $\approx 2t_c/v$, during which the longitudinal transitions $\Gamma_{\infty,\epsilon} \propto (t_c/\Omega)^2$ are most effective. In the case of noise in tunnel coupling, the opposite is true, since larger t_c only slightly decreases time spent outside of the avoided crossing region, while $\Gamma_{\infty,t} \propto (v\tau/\Omega)^2$.

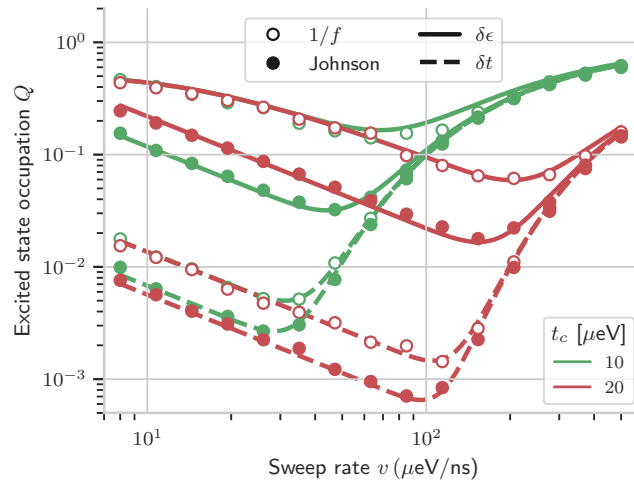

FIG. 9. Probability of occupying higher energy state after detuning sweep Q in presence of white (filled) and $1/f$ (hollow dots) classical noise in detuning/tunneling as a function of sweep rate for tunnel couplings $t_c = 10\,\mu$eV (green) and $20\,\mu$eV (red). Points correspond to numerical simulation of Schrodinger equation averaged over realization of classical noise process. Lines correspond to analytical expression $Q^{(\infty)}$ with the rates calculated according to Eq. (A13) for the noise in detunning $\delta\epsilon$ (solid) and tunnel coupling δt (dashed). For illustration, we used arbitrary parameters for detuning noise $S^\epsilon_{0.1}T/T_{0.1} = (1.5)^2\,\mu\text{eV}^2/\text{Hz}$ (1/f) and $2Jk_BT = (0.3)^2\,\mu\text{eV}^2/\text{Hz}$ (white part of Johnsons noise). The tunnel coupling fluctuations are reduced by a factor of 10, i.e., $S^\epsilon(\omega) = (10^2)S^t(\omega)$. To emulate high temperature limit, we set terminal sweep rate to $\epsilon_f = 100\,\mu$eV, which corresponds to thermal energy at $T \approx 1.2$ K.

APPENDIX B: DETAILS OF PHONON RELAXATION RATE

We now turn to evaluation of zero-temperature phonon relaxation rate in more detail. First, we show how orbital and interdot phonon-related processes emerge when using the $|\pm,\theta\rangle$ basis of eigenstates of instantaneous Hamiltonian. Next we investigate the elements for the Gaussian choice of electron wave functions and discuss the role of harmonic and Hund-Muliken approximation.

1. Interdot and orbital processes

We start with the phonon spectral density, given by Eq. (34), which predicts $S(\omega) \propto |\langle -|e^{i\mathbf{kr}}|+\rangle|^2$. We now evaluate the matrix element by plugging in the adiabatic basis given by Eqs. (3), which results in

$$\langle -,\theta|e^{i\mathbf{kr}}|+,\theta\rangle = \cos\theta\,\Re\langle L|e^{i\mathbf{kr}}|R\rangle + \Im\langle L|e^{i\mathbf{kr}}|R\rangle + \tfrac{1}{2}\sin\theta(\langle L|e^{i\mathbf{kr}}|L\rangle - \langle R|e^{i\mathbf{kr}}|R\rangle), \qquad \text{(B1)}$$

where $\tan\theta = -\epsilon/t_c$, and consecutive terms correspond to interdot ($\hat\sigma_x$, $\hat\sigma_y$) and orbital $\hat\sigma_z$ coupling in the dot basis, respectively. In the absence of large magnetic field in z direction, wave functions can be assumed real, hence $\Im\langle L|e^{i\mathbf{kr}}|R\rangle = 0$. The exact form of matrix element depends on the assumed form of wave functions, i.e., $\psi_{L/R}(\mathbf{r}) = \langle\mathbf{r}|L/R\rangle$, which will be investigated below.

2. Hund-Mulliken approximation

Before invoking the concrete form of wave function of an electron localized in a QD, let us comment on the so-called Hund-Mulliken approximation, in which one uses orthogonalized orbitals $|L/R\rangle = \mathcal{N}(|L_0/R_0\rangle - g|R_0/L_0\rangle)$ built from a bare wave function of electrons in isolated QDs: $|L_0/R_0\rangle$, with $\mathcal{N}$ being normalization constant. The parameter g is a function of the overlap $l = \langle L_0|R_0\rangle \ll 1$, with its value given by the orthogonality condition,

$$\langle L|R\rangle = \mathcal{N}^2(l - 2g + lg^2) = 0, \tag{B2}$$

from which $g = (1 - \sqrt{1-l^2})/l \sim l/2$ for $l \ll 1$. Consistently, we concentrate on leading order in g or l, according to which and $1 = \langle L|L\rangle = \mathcal{N}^2(1 - 2gl + g^2)$, we take $\mathcal{N} \approx 1$. Assuming real wave function $|L_0/R_0\rangle$, we substitute the orthogonalized states into Eq. (B1) from which we obtain

$$\begin{aligned}&\langle -|e^{i\mathbf{kr}}|+\rangle \\ &\quad\approx \cos\theta(\langle L_0|e^{i\mathbf{kr}}|R_0\rangle - g(\langle L_0|e^{i\mathbf{kr}}|L_0\rangle + \langle R_0|e^{i\mathbf{kr}}|R_0\rangle)) \\ &\quad+ \tfrac{1}{2}\sin\theta(\langle L_0|e^{i\mathbf{kr}}|L_0\rangle - \langle R_0|e^{i\mathbf{kr}}|R_0\rangle),\end{aligned} \tag{B3}$$

where in the latter term correction linear in the overlap g cancels.

3. Harmonic approximation

Finally, we substitute concrete form of isolated wave functions, and evaluate matrix element $\langle -|e^{i\mathbf{kr}}|+\rangle$. We assume the wave function is independent in all three directions ($\Psi_{L_0/R_0}(\mathbf{r}) = \psi_{L_0/R_0}(x,y)\psi_z(z)$) and has a Gaussian shape:

$$\begin{aligned}\psi_{L_0/R_0}(x,y) &= \frac{1}{\left(\pi^2 r_{xy}^4\right)^{1/4}}\exp\left(-\frac{(x \pm \Delta x/2)^2 + y^2}{2r_{xy}^2}\right), \\ \psi_z(z) &= \frac{1}{\left(\pi r_z^2\right)^{1/4}}\exp\left(-\frac{z^2}{2r_z^2}\right),\end{aligned} \tag{B4}$$

such that for the electron wave function, $\mathrm{FWHM}_x \approx 2r_{xy}$ and $\mathrm{FWHM}_z \approx 2r_z$. In such a case, Eq. (B3) reads

$$\begin{aligned}\langle -|e^{i\mathbf{kr}}|+\rangle \approx \exp&\left(-\frac{k_{xy}^2 r_{xy}^2 + k_z^2 r_z^2}{4}\right) \\ &\times\left(\cos\theta\exp\left(-\frac{\Delta x^2}{4r_{xy}^2}\right)\left(1 - \cos(k_x\Delta x/2)\right)\right. \\ &\left. - i\sin\theta\sin(k_x\Delta x/2)\right),\end{aligned} \tag{B5}$$

where we used that in harmonic approximation $g = l/2 = \frac{1}{2}e^{-\Delta x^2/4r_{xy}^2}$. Interdot and orbital relaxation are given by real and imaginary parts of the above matrix element and hence cause relaxation independently.

[1] R. Hanson, L. P. Kouwenhoven, J. R. Petta, S. Tarucha, and L. M. K. Vandersypen, Spins in few-electron quantum dots, Rev. Mod. Phys. **79**, 1217 (2007).

[2] C. Volk, A. M. J. Zwerver, U. Mukhopadhyay, P. T. Eendebak, C. J. van Diepen, J. P. Dehollain, T. Hensgens, T. Fujita, C. Reichl, W. Wegscheider, and L. M. K. Vandersypen, Loading a quantum-dot based "Qubyte" register, npj Quantum Inf. **5**, 29 (2019).

[3] F. Kuemmeth and H. Bluhm, Roadmap for gaas spin qubits, arXiv:2011.13907.

[4] W. I. L. Lawrie, H. G. J. E. N. W. Hendrickx, J. M. Boter, L. Petit, S. V. Amitonov, M. Lodari, B. Wuetz, C. Volk, S. Philips, G. Droulers, N. Kalhor, F. van Riggelen, D. Brousse, A. Sammak, L. M. K. Vandersypen, G. Scappucci, and M. Veldhorst, Quantum dot arrays in silicon and germanium, Appl. Phys. Lett. **116**, 080501 (2020).

[5] M. Veldhorst, H. G. Eenink, C. H. Yang, and A. S. Dzurak, Silicon CMOS architecture for a spin-based quantum computer, Nat. Commun. **8**, 1766 (2017).

[6] B. Buonacorsi, Z. Cai, E. B. Ramirez, K. S. Willick, S. M. Walker, Jiahao, B. D. Shaw, X. Xu, S. C. Benjamin, and J. Baugh, Network architecture for a topological quantum computer in silicon, Quantum Sci. Technol. **4**, 025003 (2019).

[7] M. F. Gonzalez-Zalba, S. de Franceschi, E. Charbon, T. Meunier, M. Vinet, and A. S. Dzurak, Scaling silicon-based quantum computing using CMOS technology: State-of-the-art, challenges and perspectives, arXiv:2011.11753.

[8] E. Chanrion, D. J. Niegemann, B. Bertrand, C. Spence, B. Jadot, J. Li, P.-A. Mortemousque, L. Hutin, R. Maurand, X. Jehl, M. Sanquer, S. De Franceschi, C. B äuerle, F. Balestro, Y.-M. Niquet, M. Vinet, T. Meunier, and M. Urdampilleta, Charge detection in an array of CMOS quantum dots, Phys. Rev. Appl. **14**, 024066 (2020).

[9] L. M. K. Vandersypen, H. Bluhm, J. S. Clarke, A. S. Dzurak, R. Ishihara, A. Morello, D. J. Reilly, L. R. Schreiber, and M. Veldhorst, Interfacing spin qubits in quantum dots and donors-hot, dense, and coherent, npj Quantum Inf. **3**, 34 (2017).

[10] P. Scarlino, D. J. van Woerkom, U. C. Mendes, J. V. Koski, A. J. Landig, C. K. Andersen, S. Gasparinetti, C. Reichl, W. Wegscheider, K. Ensslin, T. Ihn, A. Blais, and A. Wallraff, Coherent microwave-photon-mediated coupling between a semiconductor and a superconducting qubit, Nat. Commun. **10**, 3011 (2019).

[11] X. Mi, J. V. Cady, D. M. Zajac, P. W. Deelman, and J. R. Petta, Strong coupling of a single electron in silicon to a microwave photon, Science **355**, 156 (2017).

[12] M. Benito, X. Mi, J. M. Taylor, J. R. Petta, and G. Burkard, Input-output theory for spin-photon coupling in Si double quantum dots, Phys. Rev. B **96**, 235434 (2017).

[13] X. Mi, M. Benito, S. Putz, D. M. Zajac, J. M. Taylor, G. Burkard, and J. R. Petta, A coherent spin-photon interface in silicon, Nature (London) **555**, 599 (2018).

[14] N. Samkharadze, G. Zheng, N. Kalhor, D. Brousse, A. Sammak, U. C. Mendes, A. Blais, G. Scappucci, and L. M. K.

Vandersypen, Strong spin-photon coupling in silicon, Science **359**, 1123 (2018).

[15] S. Hermelin, S. Takada, M. Yamamoto, S. Tarucha, A. D. Wieck, L. Saminadayar, C. Baüerle, and T. Meunier, Electrons surfing on a sound wave as a platform for quantum optics with flying electrons, Nature (London) **477**, 435 (2011).

[16] R. P. G. McNeil, M. Kataoka, C. J. B. Ford, C. H. W. Barnes, D. Anderson, G. A. C. Jones, I. Farrer, and D. A. Ritchie, On-demand single-electron transfer between distant quantum dots, Nature (London) **477**, 439 (2011).

[17] B. Bertrand, S. Hermelin, S. Takada, M. Yamamoto, S. Tarucha, A. Ludwig, A. D. Wieck, C. Bäuerle, and T. Meunier, Fast spin information transfer between distant quantum dots using individual electrons, Nat. Nanotechnol. **11**, 672 (2016).

[18] S. Takada, H. Edlbauer, H. V. Lepage, J. Wang, P.-A. Mortemousque, G. Georgiou, C. H. W. Barnes, C. J. B. Ford, M. Yuan, P. V. Santos, X. Waintal, A. Ludwig, A. D. Wieck, M. Urdampilleta, T. Meunier, and C. Bäuerle, Sound-driven single-electron transfer in a circuit of coupled quantum rails, Nat. Commun. **10**, 4557 (2019).

[19] P.-A. Mortemousque, B. Jadot, E. Chanrion, V. Thiney, C. Bäuerle, A. Ludwig, A. D. Wieck, M. Urdampilleta, and T. Meunier, Enhanced spin coherence while displacing electron in a 2D array of quantum dots, arXiv:2101.05968.

[20] B. Jadot, P.-A. Mortemousque, E. Chanrion, V. Thiney, A. Ludwig, A. D. Wieck, M. Urdampilleta, C. Bäuerle, and T. Meunier, Distant spin entanglement via fast and coherent electron shuttling, Nat. Nanotechnol. **16**, 570 (2021).

[21] T. A. Baart, M. Shafiei, T. Fujita, C. Reichl, W. Wegscheider, and L. M. K. Vandersypen, Single-s CCD, Nat. Nanotechnol. **11**, 330 (2016).

[22] T. Fujita, T. A. Baart, C. Reichl, W. Wegscheider, and L. M. K. Vandersypen, Coherent shuttle of electron-spin states, npj Quantum Inf. **3**, 22 (2017).

[23] H. Flentje, P.-A. Mortemousque, R. Thalineau, A. Ludwig, A. D. Wieck, C. Bäuerle, and T. Meunier, Coherent long-distance displacement of individual electron spins, Nat. Commun. **8**, 501 (2017).

[24] A. R. Mills, D. M. Zajac, M. J. Gullans, F. J. Schupp, T. M. Hazard, and J. R. Petta, Shuttling a single charge across a one-dimensional array of silicon quantum dots, Nat. Commun. **10**, 1063 (2019).

[25] T. Nakajima, M. R. Delbecq, T. Otsuka, S. Amaha, J. Yoneda, A. Noiri, K. Takeda, G. Allison, A. Ludwig, A. D. Wieck, X. Hu, F. Nori, and S. Tarucha, Coherent transfer of electron spin correlations assisted by dephasing noise, Nat. Commun. **9**, 2133 (2018).

[26] C. J. van Diepen, T.-K. Hsiao, U. Mukhopadhyay, C. Reichl, W. Wegscheider, and L. M. K. Vandersypen, Electron cascade for distant spin readout, Nat. Commun. **12**, 77 (2021).

[27] J. Yoneda *et al.*, Coherent spin qubit transport in silicon, Nat. Commun. **12**, 4114 (2021).

[28] S. N. Shevchenko, S. Ashhab, and F. Nori, Landau-Zener-Stückelberg interferometry, Phys. Rep. **492**, 1 (2010).

[29] X. Li, E. Barnes, J. P. Kestner, and S. Das Sarma, Intrinsic errors in transporting a single-spin qubit through a double quantum dot, Phys. Rev. A **96**, 012309 (2017).

[30] F. Ginzel, A. R. Mills, J. R. Petta, and G. Burkard, Spin shuttling in a silicon double quantum dot, Phys. Rev. B **102**, 195418 (2020).

[31] M. Friesen, S. Chutia, C. Tahan, and S. N. Coppersmith, Valley splitting theory of SiGe/Si/SiGe quantum wells, Phys. Rev. B **75**, 115318 (2007).

[32] D. Culcer, X. Hu, and S. Das Sarma, Interface roughness, valley-orbit coupling, and valley manipulation in quantum dots, Phys. Rev. B **82**, 205315 (2010).

[33] F. A. Zwanenburg, A. S. Dzurak, A. Morello, M. Y. Simmons, L. C. L. Hollenberg, G. Klimeck, S. Rogge, S. N. Coppersmith, and M. A. Eriksson, Silicon quantum electronics, Rev. Mod. Phys. **85**, 961 (2013).

[34] X. Zhao and X. Hu, Toward high-fidelity coherent electron spin transport in a GaAs double quantum dot, Sci. Rep. **8**, 13968 (2018).

[35] X. Zhao and X. Hu, Coherent electron transport in silicon quantum dots, arXiv:1803.00749.

[36] E. Cota and S. E. Ulloa, Spin-orbit interaction and controlled singlet-triplet dynamics in silicon double quantum dots, J. Phys.: Condens. Matter **30**, 295301 (2018).

[37] S. N. Shevchenko, A. I. Ryzhov, and F. Nori, Low-frequency spectroscopy for quantum multi-level systems, Phys. Rev. B **98**, 195434 (2018).

[38] J. A. Krzywda and L. Cywiński, Adiabatic electron charge transfer between two quantum dots in presence of $1/f$ noise, Phys. Rev. B **101**, 035303 (2020).

[39] B. Buonacorsi, B. Shaw, and J. Baugh, Simulated coherent electron shuttling in silicon quantum dots, Phys. Rev. B **102**, 125406 (2020).

[40] R. K. Malla, V. Y. Chernyak, and N. A. Sinitsyn, Nonadiabatic transitions in Landau-Zener grids: Integrability and semiclassical theory, Phys. Rev. B **103**, 144301 (2021).

[41] M. Yamaguchi, T. Yuge, and T. Ogawa, Markovian quantum master equation beyond adiabatic regime, Phys. Rev. E **95**, 012136 (2017).

[42] L. Arceci, S. Barbarino, R. Fazio, and G. E. Santoro, Dissipative Landau-Zener problem and thermally assisted quantum annealing, Phys. Rev. B **96**, 054301 (2017).

[43] A. J. Leggett, S. Chakravarty, A. T. Dorsey, M. P. A. Fisher, A. Garg, and W. Zwerger, Dynamics of the dissipative two-state system, Rev. Mod. Phys. **59**, 1 (1987).

[44] S. Javanbakht, P. Nalbach, and M. Thorwart, Dissipative Landau-Zener quantum dynamics with transversal and longitudinal noise, Phys. Rev. A **91**, 052103 (2015).

[45] Z. Huang and Y. Zhao, Dynamics of dissipative Landau-Zener transitions, Phys. Rev. A **97**, 013803 (2018).

[46] D. Zueco, P. Hänggi, and S. Kohler, Landau–Zener tunnelling in dissipative circuit QED, New J. Phys. **10**, 115012 (2008).

[47] K. Saito, M. Wubs, S. Kohler, Y. Kayanuma, and P. Hänggi, Dissipative Landau-Zener transitions of a qubit: Bath-specific and universal behavior, Phys. Rev. B **75**, 214308 (2007).

[48] M. Wubs, K. Saito, S. Kohler, P. Hänggi, and Y. Kayanuma, Gauging a Quantum Heat Bath with Dissipative Landau-Zener Transitions, Phys. Rev. Lett. **97**, 200404 (2006).

[49] P. Ao and J. Rammer, Quantum dynamics of a two-state system in a dissipative environment, Phys. Rev. B **43**, 5397 (1991).

[50] V. L. Pokrovsky and D. Sun, Fast quantum noise in the Landau-Zener transition, Phys. Rev. B **76**, 024310 (2007).

[51] Y. Kayanuma and H. Nakayama, Nonadiabatic transition at a level crossing with dissipation, Phys. Rev. B **57**, 13099 (1998).

[52] P. Nalbach, Adiabatic-Markovian bath dynamics at avoided crossings, Phys. Rev. A **90**, 042112 (2014).

[53] P. Nalbach and M. Thorwart, Landau-Zener Transitions in a Dissipative Environment: Numerically Exact Results, Phys. Rev. Lett. **103**, 220401 (2009).

[54] A. Benseny and K. Mølmer, Adiabatic theorem revisited: The unexpectedly good performance of adiabatic passage, Phys. Rev. A **103**, 062215 (2021).

[55] H. Chen and D. A. Lidar, Why and When Pausing is Beneficial in Quantum Annealing, Phys. Rev. Appl. **14**, 014100 (2020).

[56] Y. Kayanuma, Nonadiabatic transitions in level crossing with energy fluctuation. I. Analytical investigations, J. Phys. Soc. Jpn. **53**, 108 (1984).

[57] Y. Kayanuma, Stochastic theory for nonadiabatic level crossing with fluctuating off-diagonal coupling, J. Phys. Soc. Jpn. **54**, 2037 (1985).

[58] A. Dodin, S. Garmon, L. Simine, and D. Segal, Landau-Zener transitions mediated by an environment: Population transfer and energy dissipation, J. Chem. Phys. **140**, 124709 (2014).

[59] V. L. Pokrovsky and N. A. Sinitsyn, Fast noise in the Landau-Zener theory, Phys. Rev. B **67**, 144303 (2003).

[60] Z. X. Luo and M. E. Raikh, Landau-Zener transition driven by slow noise, Phys. Rev. B **95**, 064305 (2017).

[61] R. K. Malla, E. G. Mishchenko, and M. E. Raikh, Suppression of the Landau-Zener transition probability by weak classical noise, Phys. Rev. B **96**, 075419 (2017).

[62] N. A. Sinitsyn and N. Prokof'ev, Nuclear spin bath effects on Landau-Zener transitions in nanomagnets, Phys. Rev. B **67**, 134403 (2003).

[63] J. I. Vestgarden, J. Bergli, and Y. M. Galperin, Nonlinearly driven Landau-Zener transition with telegraph noise, Phys. Rev. B **77**, 014514 (2008).

[64] M. H. S. Amin and D. V. Averin, Macroscopic Resonant Tunneling in the Presence of Low Frequency Noise, Phys. Rev. Lett. **100**, 197001 (2008).

[65] X. You, A. A. Clerk, and J. Koch, Positive- and negative-frequency noise from an ensemble of two-level fluctuators, Phys. Rev. Research **3**, 013045 (2021).

[66] T. Albash, S. Boixo, Daniel A Lidar, and Paolo Zanardi, Quantum adiabatic Markovian master equations, New J. Phys. **14**, 123016 (2012).

[67] M. Vogelsberger and D. A. Garanin, Butterfly hysteresis curve is a signature of adiabatic Landau-Zener transition, Phys. Rev. B **73**, 092412 (2006).

[68] P. Haikka and K. Molmer, Dissipative Landau-Zener level crossing subject to continuous measurement: Excitation despite decay, Phys. Rev. A **89**, 052114 (2014).

[69] A. A. Clerk, M. H. Devoret, S. M. Girvin, F. Marquardt, and R. J. Schoelkopf, Introduction to quantum noise, measurement, and amplification, Rev. Mod. Phys. **82**, 1155 (2010).

[70] V. Langrock, N. Focke, I. Seidler, L. R. Schreiber, J. A. Krzywda, L. Cywiński *et al.*, Proposal of a scalable quantum bus device for coherent mid-range qubit transfer in disordered Si/SiGe/SiO2 (unpublished).

[71] M. Demirplak and S. A. Rice, Adiabatic population transfer with control fields, J. Phys. Chem. A **107**, 9937 (2003).

[72] R. J. Schoelkopf, A. A. Clerk, S. M. Girvin, K. W. Lehnert, and M. H. Devoret, Qubits as spectrometers of quantum noise, in *Quantum Noise in Mesoscopic Physics*, edited by Y. V. Nazarov (Kluwer, Dordrecht, 2003), pp. 175–203.

[73] E. Paladino, Y. M. Galperin, G. Falci, and B. L. Altshuler, $1/f$ noise: Implications for solid-state quantum information, Rev. Mod. Phys. **86**, 361 (2014).

[74] F. Marquardt and V. A. Abalmassov, Spin relaxation in a quantum dot due to Nyquist noise, Phys. Rev. B **71**, 165325 (2005).

[75] P. Huang and X. Hu, Spin relaxation due to charge noise, Phys. Rev. B **89**, 195302 (2014).

[76] U. Weiss, *Quantum Dissipative Systems* (World Scientific, Singapore, 1999).

[77] A. Hollmann, T. Struck, V. Langrock, A. Schmidbauer, F. Schauer, T. Leonhardt, K. Sawano, H. Riemann, N. V. Abrosimov, D. Bougeard, and L. R. Schreiber, Large, Tunable Valley Splitting and Single-Spin Relaxation Mechanisms in a Si/Si_xGe_{1-x} Quantum Dot, Phys. Rev. Appl. **13**, 034068 (2020).

[78] P. Szańkowski, G. Ramon, J. Krzywda, D. Kwiatkowski, and Ł. Cywiński, Environmental noise spectroscopy with qubits subjected to dynamical decoupling, J. Phys.: Condens. Matter **29**, 333001 (2017).

[79] Y.-C. Yang, S. N. Coppersmith, and M. Friesen, Achieving high-fidelity single-qubit gates in a strongly driven charge qubit with 1/f charge noise, npj Quantum Inf. **5**, 12 (2019).

[80] X. Mi, S. Kohler, and J. R. Petta, Landau-Zener interferometry of valley-orbit states in Si/SiGe double quantum dots, Phys. Rev. B **98**, 161404(R) (2018).

[81] T. Struck, A. Hollmann, F. Schauer, O. Fedorets, A. Schmidbauer, K. Sawano, H. Riemann, N. V. Abrosimov, Ł. Cywiński, D. Bougeard, and L. R. Schreiber, Low-frequency spin qubit energy splitting noise in highly purified 28Si/SiGe, npj Quantum Inf. **6**, 40 (2020).

[82] B. M. Freeman, J. S. Schoenfield, and H. Jiang, Comparison of low frequency charge noise in identically patterned Si/SiO_2 and Si/SiGe quantum dots, Appl. Phys. Lett. **108**, 253108 (2016).

[83] E. J. Connors, J. J. Nelson, H. Qiao, L. F. Edge, and J. M. Nichol, Low-frequency charge noise in Si/SiGe quantum dots, Phys. Rev. B **100**, 165305 (2019).

[84] L. Petit, J. M. Boter, H. G. J. Eenink, G. Droulers, M. L. V. Tagliaferri, R. Li, D. P. Franke, K. J. Singh, J. S. Clarke, R. N. Schouten, V. V. Dobrovitski, L. M. K. Vandersypen, and M. Veldhorst, Spin Lifetime and Charge Noise in Hot Silicon Quantum Dot Qubits, Phys. Rev. Lett. **121**, 076801 (2018).

[85] J.-S. Kim, T. M. Hazard, A. A. Houck, and S. A. Lyon, A low-disorder metal-oxide-silicon double quantum dot, Appl. Phys. Lett. **114**, 043501 (2019).

[86] L. Kranz, S. K. Gorman, B. Thorgrimsson, Y. He, D. Keith, J. G. Keizer, and M. Y. Simmons, Exploiting a single crystal environment to minimize the charge noise on qubits in silicon, Adv. Mater. **32**, 2003361 (2020).

[87] E. J. Connors, J. J. Nelson, and J. M. Nichol, Charge-noise spectroscopy of Si/SiGe quantum dots via dynamically-decoupled exchange oscillations, arXiv:2103.02448.

[88] R. M. Jock, N. T. Jacobson, M. Rudolph, D. R. Ward, M. S. Carroll, and D. R. Luhman, A silicon singlet-triplet qubit driven by spin-valley coupling, arXiv:2102.12068.

[89] O. E. Dial, M. D. Shulman, S. P. Harvey, H. Bluhm, V. Umansky, and A. Yacoby, Charge Noise Spectroscopy Using Coherent Exchange Oscillations in a Singlet-Triplet Qubit, Phys. Rev. Lett. **110**, 146804 (2013).

[90] P. Cerfontaine, T. Botzem, J. Ritzmann, S. S. Humpohl, A. Ludwig, D. Schuh, D. Bougeard, A. D. Wieck, and H. Bluhm, Closed-loop control of a GaAs-based singlet-triplet spin qubit with 99.5% gate fidelity and low leakage, Nat. Commun. **11**, 4144 (2020).

[91] L. Petit, H. G. J. Eenink, M. Russ, W. I. L. Lawrie, N. W. Hendrickx, S. G. J. Philips, J. S. Clarke, L. M. K. Vandersypen, and M. Veldhorst, Universal quantum logic in hot silicon qubits, Nature (London) **580**, 355 (2020).

[92] K. W. Chan, W. Huang, C. H. Yang, J. C. C. Hwang, B. Hensen, T. Tanttu, F. E. Hudson, K. M. Itoh, A. Laucht, A. Morello, and A. S. Dzurak, Assessment of a Silicon Quantum Dot Spin Qubit Environment Via Noise Spectroscopy, Phys. Rev. Appl. **10**, 044017 (2018).

[93] G. Ramon and X. Hu, Decoherence of spin qubits due to a nearby charge fluctuator in gate-defined double dots, Phys. Rev. B **81**, 045304 (2010).

[94] P. Szańkowski, M. Trippenbach, and Ł. Cywiński, Spectroscopy of cross correlations of environmental noises with two qubits, Phys. Rev. A **94**, 012109 (2016).

[95] Z. Shi, C. B. Simmons, D. R. Ward, J. R. Prance, R. T. Mohr, T. S. Koh, J. K. Gamble, X. Wu, D. E. Savage, M. G. Lagally, M. Friesen, S. N. Coppersmith, and M. A. Eriksson, Coherent quantum oscillations and echo measurements of a Si charge qubit, Phys. Rev. B **88**, 075416 (2013).

[96] M. Raith, P. Stano, F. Baruffa, and J. Fabian, Theory of Spin Relaxation in Two-Electron Lateral Coupled Quantum Dots, Phys. Rev. Lett. **108**, 246602 (2012).

[97] P. Y. Yu and M. Cardona, *Fundamentals of Semiconductors*, Graduate Texts in Physics (Springer, Berlin, 2010).

[98] G. Burkard, D. Loss, and D. P. DiVincenzo, Coupled quantum dots as quantum gates, Phys. Rev. B **59**, 2070 (1999).

[99] Q. Li, L. Cywiński, D. Culcer, X. Hu, and S. Das Sarma, Exchange coupling in silicon quantum dots: Theoretical considerations for quantum computation, Phys. Rev. B **81**, 085313 (2010).

[100] Z.-H. Wang and S. Takahashi, Spin decoherence and electron spin bath noise of a nitrogen-vacancy center in diamond, Phys. Rev. B **87**, 115122 (2013).

[101] H. G. J. Eenink, L. Petit, W. I. L. Lawrie, J. S. Clarke, L. M. K. Vandersypen, and M. Veldhorst, Tunable coupling and isolation of single electrons in silicon metal-oxide-semiconductor quantum dots, Nano Lett. **19**, 8653 (2019).

[102] F. K. Malinowski, F. Martins, Ł. Cywiński, M. S. Rudner, P. D. Nissen, S. Fallahi, G. C. Gardner, M. J. Manfra, C. M. Marcus, and F. Kuemmeth, Spectrum of the nuclear environment for GaAs spin qubits, Phys. Rev. Lett. **118**, 177702 (2017).

[103] V. Srinivasa, K. C. Nowack, M. Shafiei, L. M. K. Vandersypen, and J. M. Taylor, Simultaneous Spin-Charge Relaxation in Double Quantum Dots, Phys. Rev. Lett. **110**, 196803 (2013).

[104] K. Wang, C. Payette, Y. Dovzhenko, P. W. Deelman, and J. R. Petta, Charge Relaxation in a Single-Electron Si/SiGe Double Quantum Dot, Phys. Rev. Lett. **111**, 046801 (2013).

[105] J. Medford, J. Beil, J. M. Taylor, E. I. Rashba, H. Lu, A. C. Gossard, and C. M. Marcus, Quantum-Dot-Based Resonant Exchange Qubit, Phys. Rev. Lett. **111**, 050501 (2013).

[106] M. Abramowitz and I. A. Stegun, *Handbook of Mathematical Functions with Formulas, Graphs, and Mathematical Tables* (Dover Publications, New York, 1965).

[107] K. Ono, T. Mori, and S. Moriyama, High-temperature operation of a silicon qubit, Sci. Rep. **9**, 469 (2019).

[108] L. Petit, M. Russ, H. G. J. Eenink, W. I. L. Lawrie, J. S. Clarke, L. M. K. Vandersypen, and M. Veldhorst, High-fidelity two-qubit gates in silicon above one Kelvin, arXiv:2007.09034.

[109] C. H. Yang, R. C. C. Leon, J. C. C. Hwang, A. Saraiva, T. Tanttu, W. Huang, J. Camirand Lemyre, K. W. Chan, K. Y. Tan, F. E. Hudson, K. M. Itoh, A. Morello, M. Pioro-Ladrière, A. Laucht, and A. S. Dzurak, Operation of a silicon quantum processor unit cell above one kelvin, Nature (London) **580**, 350 (2020).

[110] E. A. Chekhovich, M. N. Makhonin, A. I. Tartakovskii, A. Yacoby, H. Bluhm, K. C. Nowack, and L. M. K. Vandersypen, Nuclear spin effects in semiconductor quantum dots, Nat. Mater. **12**, 494 (2013).

[111] L. V. C. Assali, H. M. Petrilli, R. B. Capaz, B. Koiller, X. Hu, and S. Das Sarma, Hyperfine interactions in silicon quantum dots, Phys. Rev. B **83**, 165301 (2011).

[112] B. M. Maune, M. G. Borselli, B. Huang, T. D. Ladd, P. W. Deelman, K. S. Holabird, A. A. Kiselev, I. Alvarado-Rodriguez, R. S. Ross, A. E. Schmitz, M. Sokolich, C. A. Watson, M. F. Gyure, and A. T. Hunter, Coherent singlet-triplet oscillations in a silicon-based double quantum dot, Nature (London) **481**, 344 (2012).

[113] E. Kawakami, P. Scarlino, D. R. Ward, F. R. Braakman, D. E. Savage, M. G. Lagally, M. Friesen, S. N. Coppersmith, M. A. Eriksson, and L. M. K. Vandersypen, Electrical control of a long-lived spin qubit in a Si/SiGe quantum dot, Nat. Nanotechnol. **9**, 666 (2014).

[114] J. Yoneda, K. Takeda, T. Otsuka, T. Nakajima, M. R. Delbecq, G. Allison, T. Honda, T. Kodera, S. Oda, Y. Hoshi, N. Usami, K. M. Itoh, and S. Tarucha, A quantum-dot spin qubit with coherence limited by charge noise and fidelity higher than 99.9%, Nat. Nanotechnol. **13**, 102 (2018).